


Article

A Simulation Analysis of the Stability of Tall and Collapse-Prone Stopes: A Case Study of the Dongguashan Copper Mine

Qinli Zhang ¹, Mingjian Huang ^{1,2,*}  and Jiang Guo ¹ 

¹ School of Resources and Safety Engineering, Central South University, Changsha 410083, China; zhangqinlicn@126.com (Q.Z.); guojiang@csu.edu.cn (J.G.)

² Hunan Lianshao Construction Engineering (Group) Co., Ltd., Changsha 410000, China

* Correspondence: h_mj@163.com

Abstract: This study conducts a simulation analysis of the stability of tall and collapse-prone stopes at the Dongguashan copper mine, using the FLAC3D-3.0 software to investigate the stress distribution and deformation behavior of geological materials under different working conditions, providing an effective means of addressing complex mechanical issues in geotechnical engineering. In this paper, the stability of the tall stopes in the Dongguashan mining area was analyzed through numerical simulations using the FLAC3D finite difference method. First, a three-dimensional numerical model of the tall stopes was established based on the actual conditions of the mining area, simulating the mining conditions and environment. Next, the stress distribution, displacement variation, and potential instability zones under different mining schemes were studied, with a comparative analysis conducted between traditional mining methods and optimized schemes to clarify their respective advantages and disadvantages. Finally, based on the simulation results, the most suitable mining scheme for the area was identified, aimed at reducing the risk of stope collapse and improving the overall stability and safety of the mine. The findings provide technical support for the design and support of tall stopes in deep deposits and offer important reference points for mine safety management.

Keywords: tall stopes; collapse; stability analysis; numerical simulation; FLAC3D



Citation: Zhang, Q.; Huang, M.; Guo, J. A Simulation Analysis of the Stability of Tall and Collapse-Prone Stopes: A Case Study of the Dongguashan Copper Mine. *Appl. Sci.* **2024**, *14*, 10608. <https://doi.org/10.3390/app142210608>

Academic Editor: Yosoon Choi

Received: 10 October 2024

Revised: 8 November 2024

Accepted: 12 November 2024

Published: 18 November 2024



Copyright: © 2024 by the authors. Licensee MDPI, Basel, Switzerland. This article is an open access article distributed under the terms and conditions of the Creative Commons Attribution (CC BY) license (<https://creativecommons.org/licenses/by/4.0/>).

1. Introduction

As mineral resources are extracted at increasing depths, tall stopes in underground mines face increasingly complex stress conditions and unstable rock mass structures. These unfavorable factors significantly heighten the risk of stope collapse, posing serious safety hazards to mining operations [1]. Particularly in deep shafts with high stress environments, the issue of stope stability becomes more prominent, severely threatening both the safe production and resource development of mines [2,3]. Thus, effectively assessing and enhancing the stability of tall stopes has become a critical topic in current mining engineering. Researching the mechanisms of stope instability and optimizing mining schemes not only helps reduce the risk of collapse and ensure operational safety, but also improves mining efficiency and resource utilization, making this of both theoretical and practical significance [4].

Currently, researchers both domestically and internationally have conducted extensive studies on the instability mechanisms of high-stability mining faces. This instability is influenced by various factors, including the mechanical properties of the surrounding rock, mining methods, in situ stress conditions, and groundwater levels [5,6]. The interaction of these factors complicates the evaluation of stope stability [7–10]. In response, researchers have widely explored stope stability through theoretical models and numerical simulations, yielding valuable results. The limit equilibrium theory was an important early tool for studying the stability of tall stopes, evaluating the risk of stope failure by analyzing the balance conditions of potential sliding surfaces and forces [11]. Block theory, by establishing a block model of the underground rock mass, analyzes the sliding and rotational

instability of block structures, providing a theoretical foundation for studying structural instability in stopes [12]. Fracture mechanics has been widely applied in instability studies of underground stopes, especially in analyzing fracture propagation within rock masses and its impact on stability [13]. In addition, models based on elastic theory [14], plastic theory [15], and energy theory [16] have also been used.

Traditional methods of stope stability analysis primarily rely on theoretical models, but these approaches often struggle to accurately reflect real-world conditions when dealing with complex rock masses and uneven stress distributions. In recent years, the development of numerical simulation technologies has provided new avenues for analyzing the stability of underground stopes [17–20]. Numerical simulations can accurately replicate the complex stress–strain states and failure processes of rock masses, offering critical insights for engineering design and risk assessment. Various numerical methods have been applied in underground stope studies [21], including the finite element method (FEM) [22], discrete element method (DEM) [23], and finite difference method (FDM) [24], yielding numerous research findings. The finite element method (FEM) is currently one of the most commonly used numerical simulation techniques, typically suitable for handling deformation characteristics and stability under complex geometries and boundary conditions. It can provide high-accuracy results, especially excelling in static and quasi-static analyses. Peng et al. [25] conducted a numerical simulation study using PLAXIS2D finite element analysis software to investigate the structural parameter scheme of the mining area and the waste rock filling scheme. By analyzing the displacement variation, surrounding rock stress distribution, and plastic zone, they determined the optimal structural parameters for the mining area. However, its computational cost is relatively high, and it requires significant computational resources. The discrete element method (DEM) is widely used to simulate the movement and interaction of particles or blocks within fractured rock masses [26]. The DEM can capture local failure processes, such as crack propagation and block sliding within the rock mass, which is particularly important for studying instability in complex underground mining areas. However, this method may not perform as well as finite difference methods when dealing with the stability analysis of continuous media. The finite difference method (FDM) is another commonly used numerical simulation technique, especially suitable for simulating deformation and fluid flow problems in continuous media [27,28]. This method can effectively address nonlinear problems, performing particularly well in the dynamic analysis of stress and deformation changes. Moreover, the FDM is relatively straightforward to implement computationally, making it especially suitable for simulating the stability of rock masses in deep, high-stress environments. At the same time, FLAC3D, a commercial software based on the FDM, is commonly used for stope stability studies [29,30]. Ren et al. [31] used the FLAC3D finite difference analysis software to simulate the original in situ stress distribution of a test stope, analyzing the effects of rectangular, elliptical, and butterfly-arched stope cross sections on stope stability, ultimately identifying the optimal stope shape. Idris et al. [32] conducted a series of numerical analyses using FLAC to study the stability of open-pit stopes. In addition, An et al. [33] introduced the combined/hybrid finite–discrete element method (FDEM) and validated its application for slope stability analysis. The study primarily focused on the contact interactions of discrete bodies and the transition between continuum and discontinuum.

With the improvements in computational power, three-dimensional numerical simulation techniques have become increasingly widespread in the stability analysis of underground stopes [34,35]. Three-dimensional models can more accurately describe the geometric shapes of stopes and the distribution of stress fields, overcoming the limitations of two-dimensional simulations. Tao et al. [36] addressed the stability issues of caving method stopes by using three-dimensional finite element methods to conduct numerical simulations of various stope structural parameters. They primarily analyzed the displacement of the roof and the principal stresses during the excavation and ore recovery processes, concluding that larger structural parameters result in greater stability for the stope compared to smaller parameters. By establishing a three-dimensional model and integrating

the mechanical properties of the rock mass with the mining conditions, it is possible to more precisely simulate the stress changes, deformation patterns, and potential failure modes of the stope. This is especially important in the complex working environments of underground mines, where numerical simulations can comprehensively consider multiple factors, providing scientific foundations to guide engineering design and construction.

This study focuses on a copper mine in Anhui, systematically analyzing the stability of tall, collapse-prone stopes in underground mines using the FLAC3D finite difference method. By establishing a numerical model of the underground stope and integrating actual working conditions, this study simulates the stress distribution, deformation characteristics, and potential instability zones under various conditions. The findings not only provide technical support for stope design and support systems but also serve as an important reference material for mine safety management.

2. Engineering Background and Numerical Simulation Scheme

2.1. Engineering Background

The Dongguashan deposit is located in the deep part of the Shizishan mining area and is a large skarn-type copper deposit. The main ore body extends 1810 m in length, with an average width of 500 m, and is buried at depths ranging from -690 to -1000 m. The copper metal reserves exceed 1 million tons, with a copper grade of 1.02% and a sulfur content of 17.6%. The roof of the ore body is primarily composed of marble, while the floor consists of sandstone and quartz diorite. The ore is mainly composed of copper skarn, serpentine, and magnetite. The mining conditions of the deposit are unique, characterized by deep shafts, high stress (30–38 MPa), high temperatures (30–39 °C), and a tendency for rock bursts.

In response to these conditions, the Dongguashan deposit employs a staged mining process involving the use of temporary isolation pillars, large panels, and high production capacity with subsequent backfilling after void creation. Every 100 m along the ore body, a panel is delineated, reserving an 18 m isolation pillar within each panel. The mining process is conducted in three steps: the first step involves mining the ore room and performing full tailings cemented backfill; the second step is the extraction of the isolation pillar, which was initially planned to use full tailings non-cemented backfill but was later changed to a low ash-to-sand ratio of cemented backfill; and the third step involves mining the isolation pillar of the panel using full tailings sand or a low ash-to-sand ratio of cemented backfill. The ore volumes extracted in each step account for 42%, 38%, and 20% of the total reserves, respectively. Currently, the mine has entered the late stage of extraction, focusing on mining the ore body and isolation pillars north of the 60 line. As the number of isolation pillar stopes increases, the complexity and difficulty of mining have significantly risen, leading to challenges in maintaining a stable and high production. Some pillar stopes have experienced wall rock collapse and over-extraction due to the structural characteristics of the ore body, secondary joints, fractures, faults, and blasting factors, resulting in remaining pillar thicknesses of less than 10 m, which pose safety hazards and can even lead to resource wastage due to the inability to extract. This is especially true for the third step involving the isolation pillar stopes, which are surrounded on three sides by backfill. The ore body, surrounding rock, and roof experience repeated disturbances from the blasting dynamic loads, weakening the stability and increasing the difficulty of production, blasting, and safety control. Therefore, the effective control of stability during the blasting process of each step is crucial, directly impacting the safety and efficiency of the extraction, loss and dilution rates, and the stability of the mine output and economic benefits. A stability analysis and simulation of these tall, collapse-prone stopes are particularly necessary.

2.2. Numerical Simulation Scheme and Simulation Steps

The purpose of the stope stability analysis is to optimize the structural parameters of the tall, collapse-prone stopes located north of the 60 line in the Dongguashan deposit. Based on the profile of the stope at the 60 line, which mainly includes stopes 60-2# to 60-28#,

this study uses the 61 line profile as a reference to establish a slope model that closely aligns with the actual conditions for the theoretical and numerical simulation analyses. Given that the Dongguashan ore body is buried at a considerable depth and that the structural stress in the mining area is complex due to factors such as folding structures, an analysis of the original rock stress testing was conducted prior to the numerical simulation. The results of the original rock stress testing are presented in Table 1.

Table 1. Results of original rock stress testing.

Middle Section/m	Principal Stress/Mpa			Inclination of Principal Stress/°			Azimuth of Principal Stress/°		
	σ_1	σ_2	σ_3	α_1	α_2	α_3	β_1	β_2	β_3
−280	19.3	15.6	12.3	18.4	27.1	56.4	247.3	147.6	7.3
−460	26.08	9.92	9.72	6.13	5.22	81.81	241.2	150.63	20.47
	22.44	12.91	10.99	3.08	83.56	5.08	53.81	172.17	323.5
−730	32.75	12.23	8.49	2.25	25.81	64.08	48.31	317.22	142.95
	34.33	16.47	13.84	6.37	44.39	44.9	248.42	152.13	344.81
−910	38.1	33.1	31.1	22.7	19.9	59	249.6	150.9	23.7

The rock mass in the Dongguashan mining section is layered, and, to simplify the model, the average mechanical parameters based on the properties of the layered surrounding rock were calculated for the simulation data. Given the significant differences between the engineering mechanical properties of the in situ rock mass and the results from laboratory tests, it was necessary to apply a reduction process to the laboratory test results before utilizing them in the numerical simulation.

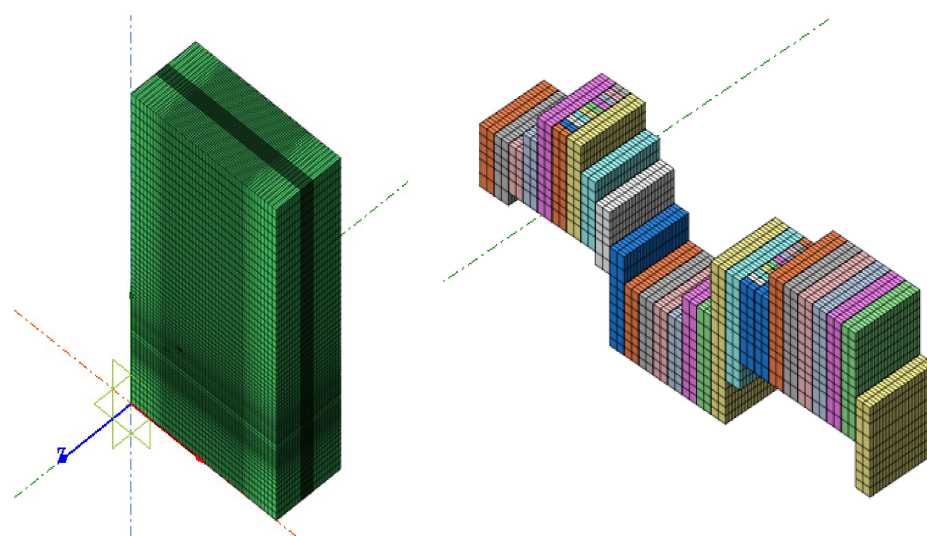
This study is based on engineering geological surveys and the RQD values of the ore body and roof rock. A specific reduction method was employed to calculate the reduced mechanical parameters of the rock mass. According to the geological variations of the rock mass at the 60 line of Dongguashan and field investigations, combined with rock classification standards, the average joint spacing was determined to be between 0.6 and 2 m. The M. Georgi method was used for the reduction, resulting in a reduction factor of 0.1 for the shear strength parameters (cohesion c and internal friction angle φ). The deformation parameters of the rock mass include the elastic modulus and Poisson's ratio, with the Poisson's ratio being used directly from the test values without reduction. For the compressive and tensile strength of the rock mass, the literature recommends using a cracking coefficient for reduction. This study did not conduct elastic wave testing, so the cracking reduction coefficient was chosen based on empirical values. Given that the integrity of the rock mass north of the 60 line in Dongguashan differs significantly from earlier assessments, with some areas being more fractured and forming blocky rock masses, a reduction coefficient of 0.45 was selected for the blocky and fractured rock masses.

After reducing the physical parameters, it was necessary to calculate the bulk modulus and shear modulus. In FLAC3D, the deformation parameters no longer use the elastic modulus E and Poisson's ratio ν but instead utilize the bulk modulus K and the shear modulus G , which represent the material's resistance to volumetric deformation and shear deformation, respectively. In practical applications, the deformation parameters typically provided are E and ν , which can be converted to K and G using the formulas $K = E/3(1 - 2\nu)$ and $G = E/2(1 + \nu)$. The slope in the Dongguashan mining section consists of three extraction steps, with different fill material proportions used after each step. Based on the actual filling conditions of the first and second steps, combined with the data on the filling material's mechanical parameters from domestic and international sources, the parameters for the fill material selected for the numerical simulation were determined. The final physical and mechanical parameters for the numerical simulation are presented in Table 2.

Table 2. Physical and mechanical parameters for numerical simulation of rock and fill material in Dongguashan.

Type	Density ρ (g/cm ³)	Cohesion c (MPa)	Internal Friction Angle φ (°)	Tensile Strength (MPa)	Bulk Modulus/GPa	Shear Modulus/GPa
Surrounding Rock	2.71	2.61	34.5	2.82	9.64	4.25
Copper Ore Body	3.97	3.89	41.1	3.62	13.2	6.72
Fill Material (1:6)	1.83	0.546	35.70	0.40	0.32	0.24
Fill Material (1:10)	1.74	0.189	27.27	0.10	0.08	0.06

This study uses the 61 line profile as a reference to establish a stope model that closely matches the actual conditions of the mining area. The dimensions of the model are $X \times Y \times Z = 900 \text{ m} \times 400 \text{ m} \times 1000 \text{ m}$, with the length of the stope model set at 80 m, the width at 18 m, and the height determined based on the thickness of the ore body. Since Midas GTS employs finite element technology for mesh generation, the node and element divisions are consistent with those in FLAC3D. The conversion program MidastoFlac3D.exe facilitates the transformation of the GTS mesh model into a numerical model for FLAC3D. The final numerical model of the surrounding rock of the ore body and the ore body model for the 60 line stope are illustrated in Figure 1.

**Figure 1.** Surrounding rock model and 60 line stope model.

The stability of rock masses is influenced by various factors, particularly in mines, where the stability of the rock not only depends on its inherent characteristics but is also affected by disturbances from surrounding stope extraction. Due to the significant differences in rock stability in different areas north of the Dongguashan 60 line, a comprehensive and uniform simulation analysis is challenging. Therefore, this analysis mainly focuses on the following two aspects: through numerical simulation, the patterns of stress or displacement changes during the extraction process are identified, thereby proposing solutions to the problems encountered; and, by comparing stress and displacement, potential issues faced by the stope are analyzed. For example, for adjacent stopes, if one remains stable after extraction while the other collapses, it is possible to differentiate the stress or displacement changes to determine the values that led to the collapse.

2.3. Step-by-Step Stope Structural Arrangement Method

The main mining method for the large stopes north of the Dongguashan 60 line involves controlling the thickness of each blast in the stope direction, with the amount of explosive used for each blast kept below 5 tons. During the step-by-step extraction process, the volume of the mined-out area gradually increases until the entire stope is extracted,

followed by filling. As shown in Figure 2a, the extraction sequence for the first step of the 60 line stope advances gradually from the 62 line side to the 60 line. However, this extraction method has led to severe collapses in the mined-out areas such as 60-24#, 60-8#, and 60-12#, which affect the extraction of the adjacent second-step stopes. Although this extraction method is the primary approach for the Dongguashan deposit, it does not meet the current production demands for some tall and fragmented rock mass stopes, where the collapse of mined-out areas is significant. Considering the extraction sequence within the stope and structural factors, three optimization plans have been developed.

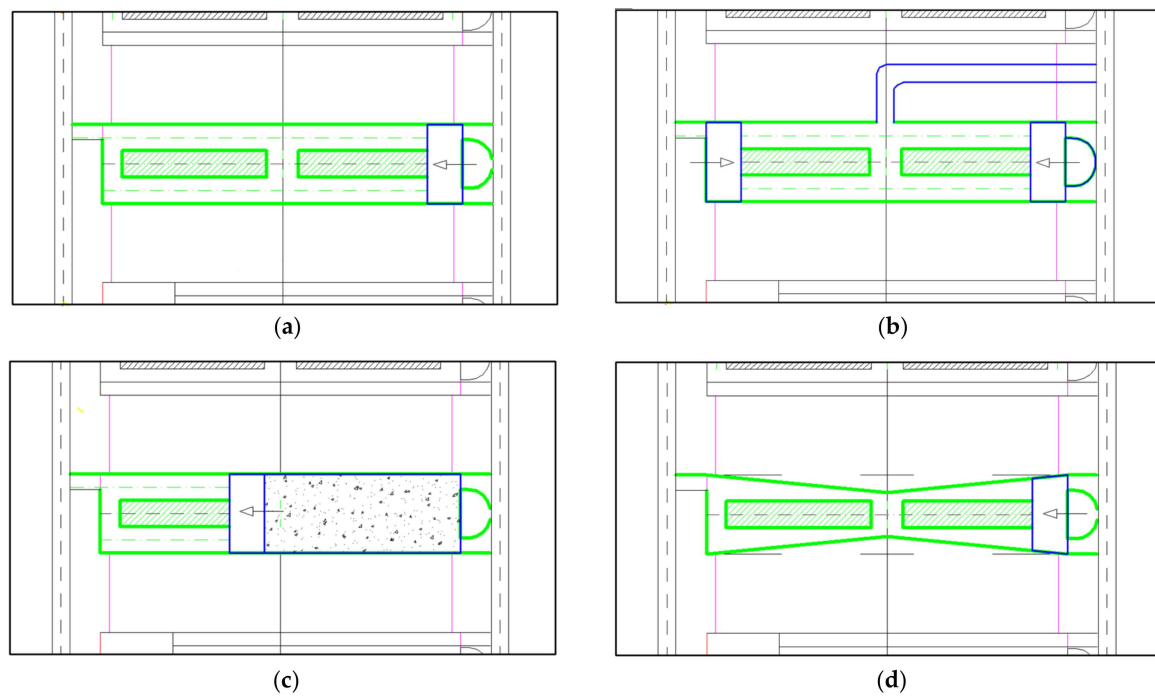


Figure 2. Schematic diagram of the extraction methods for the step one stope. (a) Extraction from one side of the stope to the other; (b) extraction from both sides to the middle; (c) extraction and filling in the stepwise extraction plan; and (d) extraction plan with reduced dimensions in the middle of the stope.

1. Plan One: Gradually Extracting from Both Sides of the Stope Towards the Center

This plan involves gradually extracting from the ends of the 60 and 62 lines towards the center, with a specified thickness for each extraction. After the blasting is completed, the ore is removed, followed by the next blasting cycle, ultimately leaving a certain thickness of mineral pillar in the center of the stope for overall extraction. This plan requires the construction of access tunnels in the two-step mineral pillars to facilitate entry and exit for the staggered blasting operations. Since the central area of the stope is the most susceptible to damage, extracting it last reduces the exposure time in this region, which is beneficial for maintaining the stability of the ore body. However, the mineral pillar at the final extraction stage has stope areas on both sides, necessitating assurances of the pillar's safety thickness to ensure the safety of blasting operations.

2. Plan Two: Extraction–Filling–Extraction

In response to the significant height of the stope north of the 60 line, this plan proposes to first extract half of the stope, followed by filling, and finally extracting the remaining ore body. This approach can reduce the exposure area and time of the stope, thereby minimizing the risk of collapse in the central area of the ore body. However, due to the extensive engineering requirements for sealing the stope and the need for at least two filling operations, this plan increases production pressure on the mine, making it unsuitable for large-scale implementation.

3. Plan Three: Reduce the Middle Size of the First-Step Stope

Based on the collapse characteristics of the stope, this plan involves reducing the extraction thickness in the middle of the first-step stope to control the collapse of the ore body on both sides of the stope. This approach divides the original exposed surface into two, forming a triangular mineral pillar that helps enhance the pillar's strength. Even if the ore body is fragmented, the primary damage location will be in the central area of the stope, allowing for the retention of a certain thickness of ore, which is beneficial for effectively protecting the second-step stope.

During the two-step extraction process, since both sides of the ore body are filled, any scheme that involves extraction from both sides toward the center requires construction within the fill body, which poses stability issues for the tunnels. Therefore, this option is excluded. The cemented fill in the first-step stope has high strength, and, when the second-step stope is extracted gradually from one side to the other, the filled body on both sides of the void can maintain good stability, with no significant collapse phenomena in the second-step void. Based on the existing extraction plans, further optimization of the internal extraction sequence is conducted. There are three main schemes for the second-step extraction:

1. Scheme One: Gradual Extraction from One Side of the Stope to the Other

This is the primary method for the second-step stope extraction in the Dongguashan deposit, as shown in Figure 3a. Considering the current state of collapse in the second-step void and the stability of the fill body, this scheme is highly feasible and has demonstrated good results. To further compare the advantages and disadvantages of other schemes, in-depth analysis of this scheme is required.

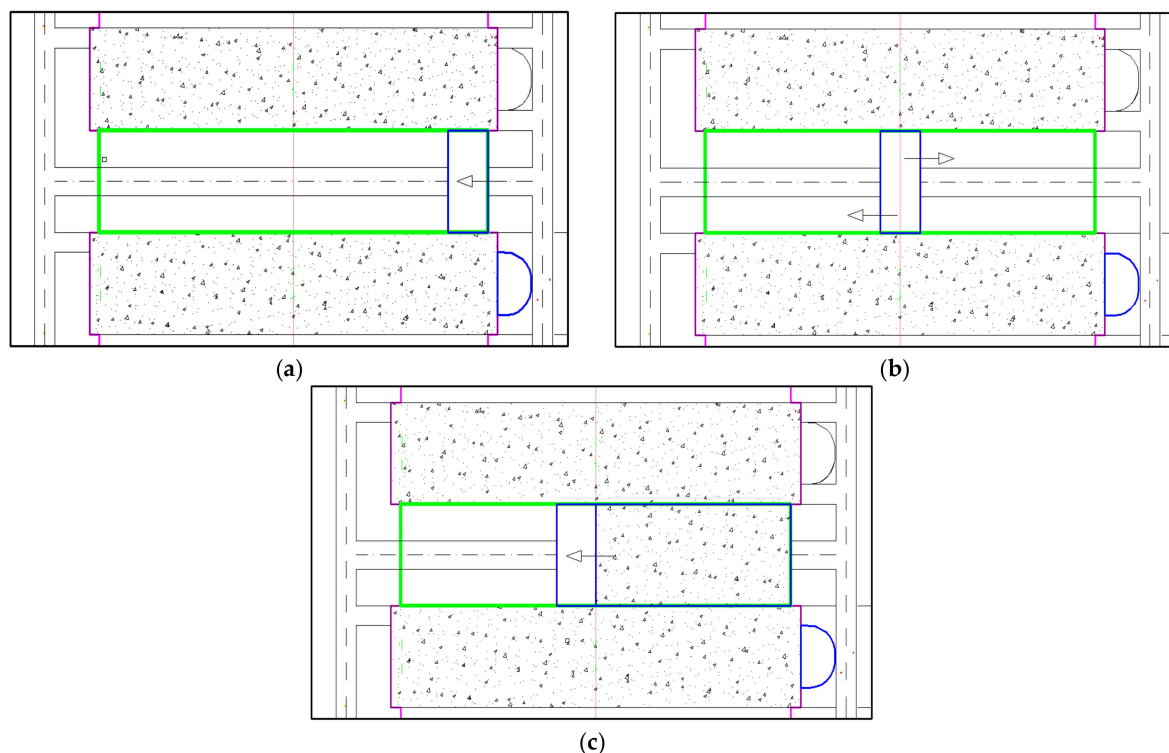


Figure 3. Schematic diagram of two-step stope extraction methods. (a) Extraction from one side to the other; (b) extraction from the middle to both sides; and (c) schematic diagram of the two-step stope extraction followed by filling and then re-extraction.

2. Scheme Two: Gradual Extraction from the Middle of the Stope to Both Sides

Due to the good strength and stability of the fill body in the Dongguashan section, this scheme ensures the safe extraction of the high stope. As illustrated in Figure 3b, during

the extraction of part of the high stope on line 58, there was no significant collapse of the fill body. Therefore, after the second-step extraction, the fill body on both sides remains stable. Extracting from the middle toward both sides can reduce the exposure time of the pillar rock on the side of the vein, which is beneficial for the effective protection of the cross-cut tunnel.

3. Scheme Three: Extraction–Filling–Extraction

As shown in Figure 3c, although the fill body has good strength, it is still relatively weak compared to the original ore rock, and some of the high stope rock north of line 60 is quite fractured. During the gradual extraction process, the rock may continue to collapse, impacting the safety of the stope extraction. With filled bodies on both sides of the second-step stope, there is a certain degree of elasticity; after the second-step extraction, the displacement of the roof will further increase. Implementing this scheme is beneficial for roof stability and provides effective support to the adjacent fill body.

3. Numerical Simulation Analysis and Demonstration of Actual Extraction Sequence in Large Stopes

3.1. Numerical Simulation Analysis of the Actual Step One Extraction Sequence in Large Stopes at the 60 Line

In the process of gradual extraction in the large stope at the 60 line, issues such as a severe collapse of the mined-out area, concentrated ground stress in the drilling chamber, and damage to support structures have emerged. To gain a deeper understanding of the stress causes behind these problems, this study conducted numerical simulations for all stopes along the 60 line. Following the actual extraction sequence of the mine and based on prior cause analysis, this study investigates the reasons for the collapse of the mined-out areas and the concentration of ground stress. By analyzing the variations in stress, displacement, and plastic zone distribution under different scenarios, the research provides support for optimizing stope structures and extraction sequences.

To understand the patterns of displacement and stress during the step one extraction process at the large stope on the 60 line, this study selected the stope sections between 60-4# and 60-12# for the extraction simulations. As shown in Figure 4, after backfilling the 60-4# stope, the simulation results for the extraction of the 60-8# stope indicate that the rock on both sides of the mined-out area is not subjected to tensile stress. The cloud map of the minimum principal stress (Figure 4b) reveals that, after the extraction of the 60-8# stope, the maximum compressive stress occurs in the 60-6# stope, reaching 33.0 MPa, indicating a stress concentration phenomenon. From the displacement cloud map (Figure 4c), the maximum displacement is located at the roof of the 60-8# mined-out area, with a maximum displacement of 6.3 cm. Additionally, the upper region on the side of the 60-8# mined-out area, near the 9# stope, also experiences some displacement, with a maximum displacement of 5 cm, although the affected area is relatively small. The plastic zone cloud map indicates that the rock on both sides of the mined-out area is subjected to shear stress, while the backfill of the 60-4# stope experiences compressive stress.

Analyzing the results from the detection of the mined-out areas, it is evident that the 60-4# stope exhibits a minimal collapse, while the 60-8# stope experiences a significant collapse towards the 9# stope. Numerical simulations show that the displacement direction of the 60-8# stope aligns with the actual direction of the collapse; however, the range of displacement is much smaller compared to that of the 60-4# stope, indicating that the primary reason for the collapse is the relatively poor stability of the rock in that region.

According to the simulation results in Figure 5, after the mining of the 60-12# working face, the distribution of the maximum principal stress indicates that the area surrounding the 60-12# void was not subjected to tensile stress. The distribution of the minimum principal stress shows that the maximum compressive stress increased to 33.8 MPa in the 60-6# working face between the 60-4# and 60-8# working faces, with a more pronounced stress concentration. Additionally, the mining of the 60-12# working face exacerbated the stress concentration in the 60-8# working face. In the 60-10# working face, located between

the 60-8# and 60-12# faces, the maximum compressive stress reached 33.7 MPa, creating a non-vertical inclined compressive stress range from the top of the 60-12# working face to the bottom of the 60-8# working face. Displacement distribution indicated that due to the significant height of the void in the 60-12# working face, the range of displacement was large, with a maximum displacement of 7.45 cm, primarily located at the upper part of the 60-12# working face near the 60-11# working face. There was also a certain degree of displacement in the lower region near the 60-11# working face, but it was smaller in extent. Plastic zone analysis revealed that the 60-12# working face was subjected to shear stress, which had reached the yield surface, but later returned to an elastic state. Combining this with the analysis of the void collapse, the 60-12# working face collapsed towards the 60-11# working face; however, the displacement cloud showed that the upper region close to the 60-11# working face had very little displacement, although serious collapse actually occurred, indicating that the collapse was primarily due to the poor stability of the rock mass.

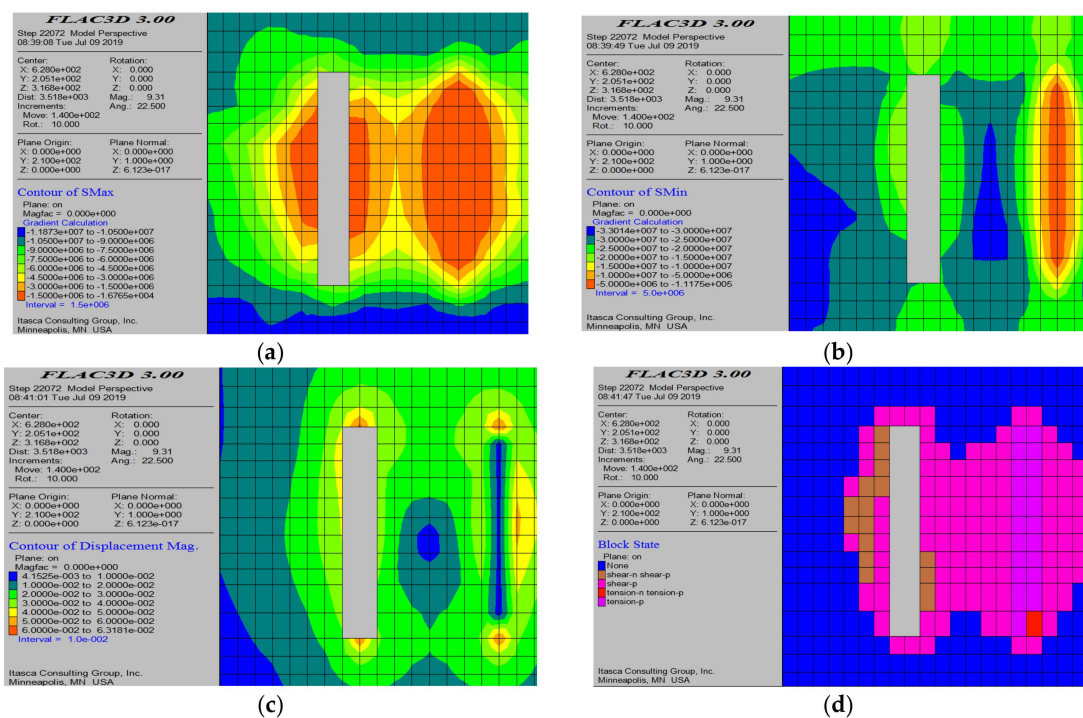


Figure 4. Simulation results after the mining of the 60-8# working face. (a) Maximum principal stress contour map; (b) minimum principal stress contour map; (c) displacement contour map; and (d) plastic zone contour map.

Field investigations indicated that the rock chamber of the 60-6# working face experienced severe collapse and the crushing failure of the intermediate pillars, mainly due to the more concentrated stress in the working face, which led to damage to the surrounding rock. This is consistent with the numerical simulation results. The misalignment of the blast holes in the 60-10# working face was analyzed through a numerical simulation, revealing a height difference of 20 m between the 60-12# and 60-8# working faces after mining, resulting in a non-vertical inclined compressive stress region that caused a significant misalignment of the blast holes. In summary, the numerical simulation aligns with the actual situation, indicating that poor rock stability is the main reason for the collapse of the void, while stress concentration leads to damage in the rock chambers and intermediate pillars.

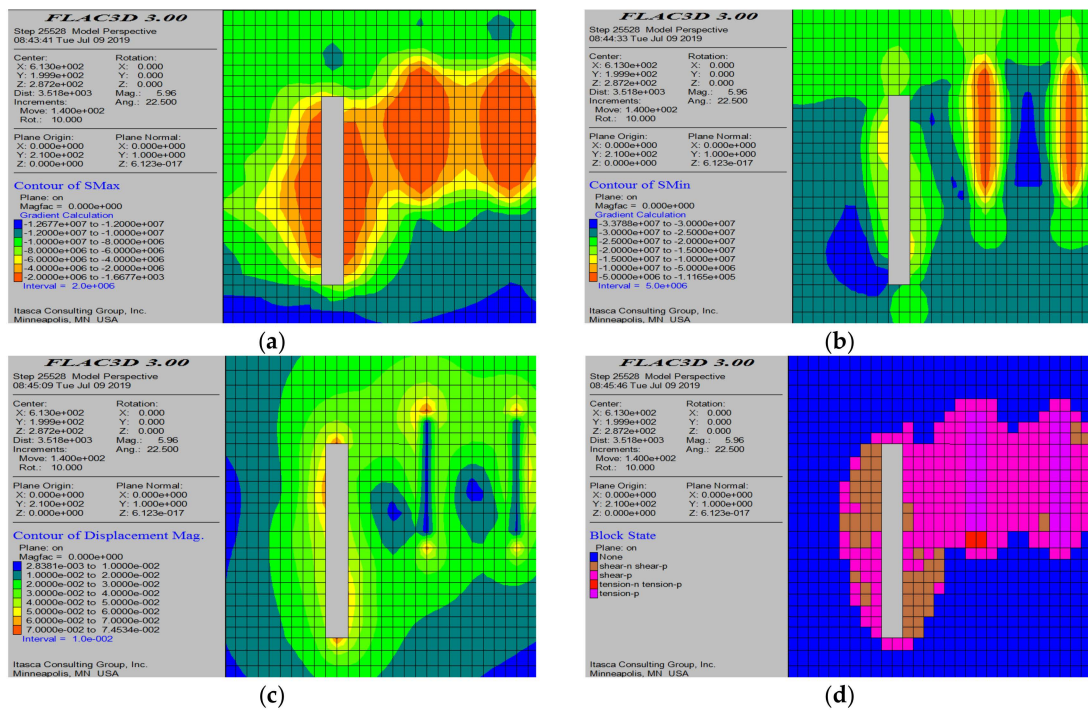


Figure 5. Simulation results of the 60-12# working face mining. (a) Maximum principal stress contour map; (b) minimum principal stress contour map; (c) displacement contour map; and (d) plastic zone contour map.

3.2. Numerical Simulation Analysis of Stepwise Mining in the 60 Line High Mining Face

To understand the changes in displacement and stress during the stepwise mining process of the high mining face on the 60 line, this study selected the stepwise mining face between 60-3# and 60-13# for a simulation analysis.

From the minimum principal stress cloud map in Figure 6b, it can be observed that, after the completion of the first-step mining, the compressive stress on the second-step pillar is relatively low, generally ranging from 17.5 to 21.0 MPa. This represents a significant reduction in compressive stress compared to the first-step mining, indicating that the stress in the 60 line mining area is largely relieved after the first-step mining is completed. The maximum principal stress cloud map in Figure 6c shows that the second-step mining area and the filling body are generally not subjected to tensile stress. When combined with the distribution of the plastic zone, it can be seen that the second-step pillar is mainly subjected to shear stress, while the filling body experiences compressive stress.

For the second-step mining, the extraction is conducted sequentially according to the actual mining sequence of “mining every third” at Dongguashan. Through a numerical simulation, the changes in stress and displacement were analyzed to assess the stability of the mined-out area after the second-step mining.

From Figure 7, after the extraction of the 60-3# working face, the maximum principal stress cloud diagram (Figure 7a) shows that only the upper part of the void is subjected to tensile stress, with a maximum tensile stress of only 0.21 MPa. The minimum principal stress cloud diagram indicates that the maximum compressive stress in the 60-5# working face is 25 MPa, which is an increase from 21 MPa prior to extraction; however, this maximum compressive stress remains relatively low and has minimal impact on the surrounding rock. In terms of the displacement of the void’s roof, the roof displacement is significant, reaching a maximum of 13.8 cm, and there is a noticeable displacement in the upper part of the ore body due to the first-stage extraction. Compared to the first stage, the roof displacement in the second stage has significantly increased. On one side of the 60-3# working face, there is filling material, while the other side consists of the original rock. The displacement from both sides indicates that the displacement of the filling material is relatively small, with

a maximum displacement of 4 cm, while the maximum displacement of the rock mass is 8.59 cm.

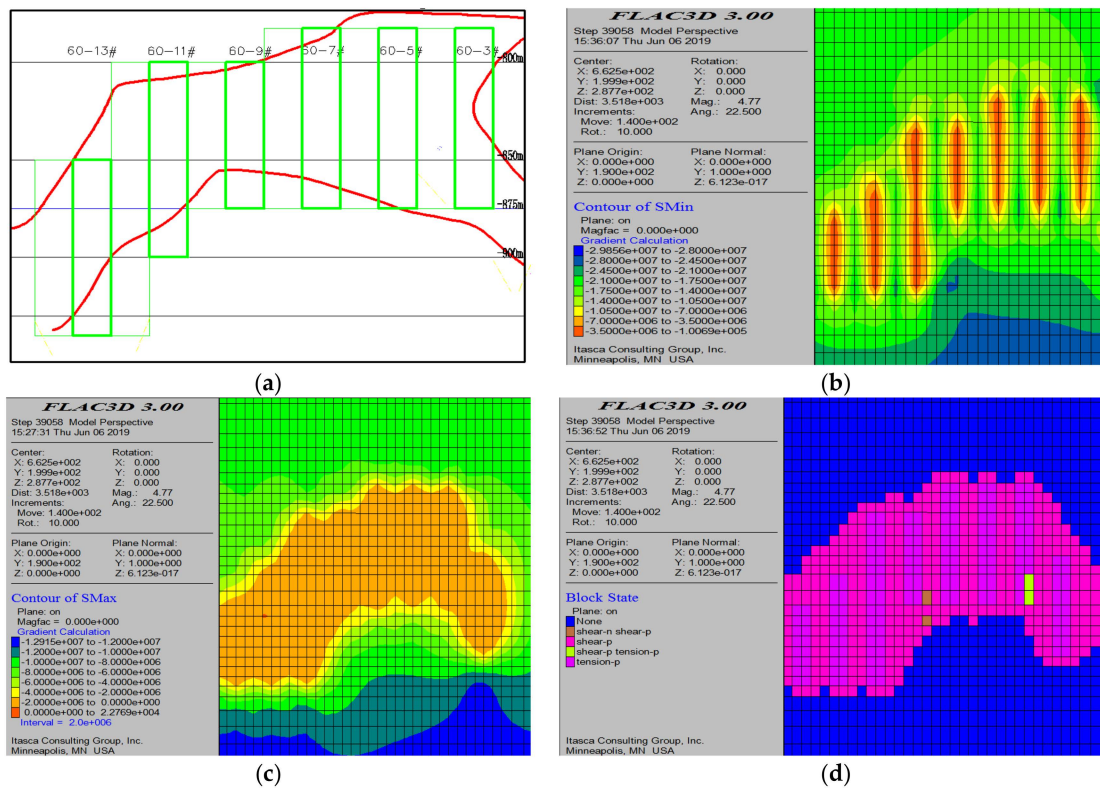


Figure 6. Stress conditions before two-step mining. (a) Simulation range area; (b) minimum principal stress cloud map; (c) maximum principal stress cloud map; and (d) plastic zone distribution.

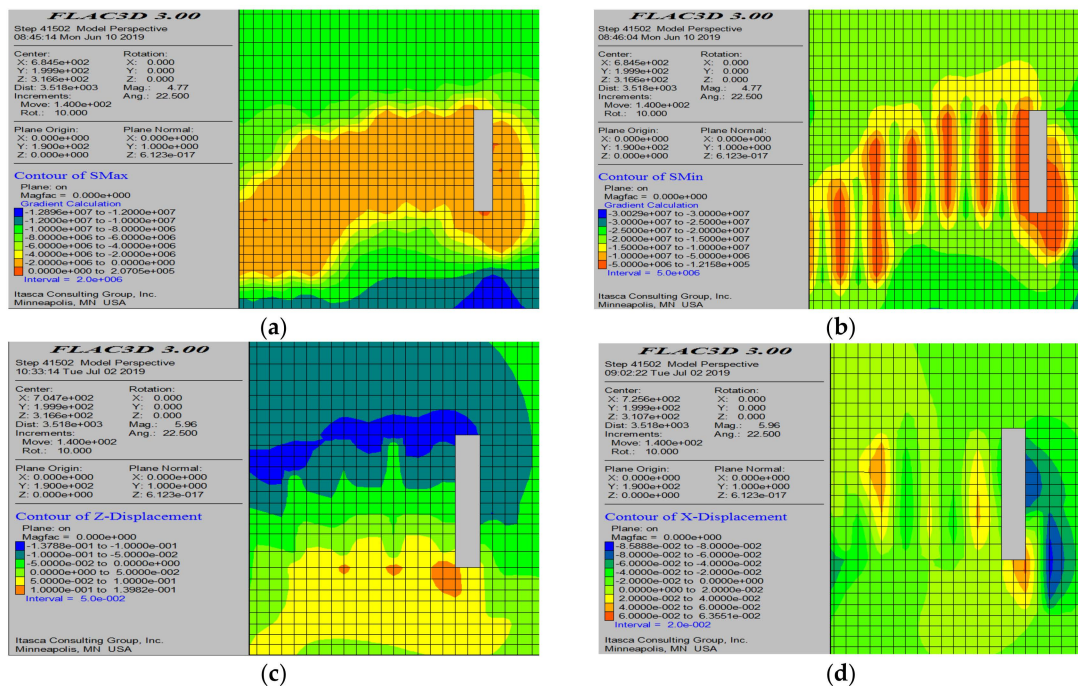


Figure 7. Simulation results after the extraction of the 60-3# working face. (a) Maximum principal stress contour map; (b) minimum principal stress contour map; (c) roof displacement contour map; and (d) displacement contour map on both sides.

From Figure 8, after the extraction of the 60-7# working face, the maximum principal stress cloud diagram (Figure 8a) shows that the range of tensile stress in the void is small, with the maximum tensile stress value increasing to 1.53 MPa. However, the small range of tensile stress results in an overall minor impact. From the minimum principal stress cloud diagram (Figure 8b), it can be observed that, after the extraction of the 60-7# working face, the maximum compressive stress in the 60-5# working face remains at 25 MPa, which is similar in range and magnitude to that observed after the extraction of the 60-3# working face. The displacement cloud diagram indicates that the maximum displacement reached 16.3 cm. There are no significant changes in the displacement of the filling materials on both sides of the 60-7# void, with the maximum displacement recorded at 6 cm.

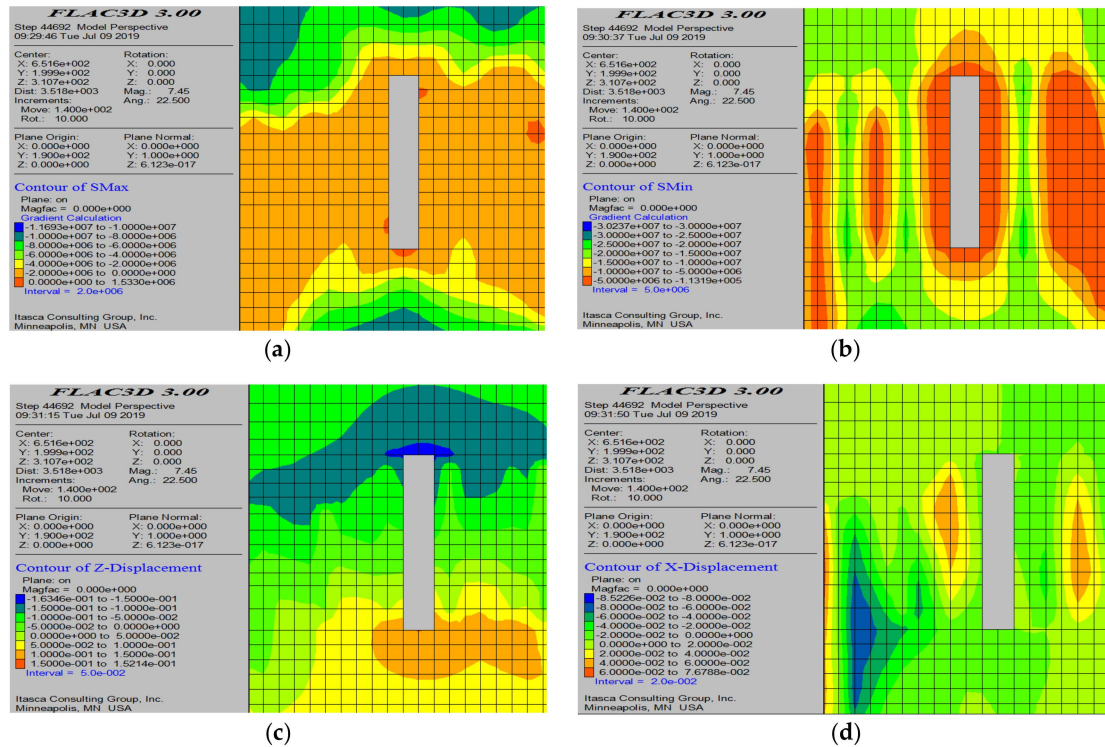


Figure 8. Simulation results after extraction of the 60-7# working face. (a) Maximum principal stress contour map; (b) minimum principal stress contour map; (c) roof displacement contour map; and (d) displacement contour map on both sides.

It is evident that, during the extraction process of the two-step working face, the stress was released after the one-step extraction, resulting in lower compressive stress values that were insufficient to compromise the integrity of the surrounding rock. In the “one-in-three” extraction process of the two-step working face, the range of the maximum tensile stress is small, and the maximum compressive stress does not vary significantly. The main change observed is the increased displacement of the void, particularly in the roof of the void, where the maximum displacement reaches 16 cm, while the filling materials on both sides exhibit a displacement range of 4–6 cm.

Despite the substantial displacement of the roof in the two-step void, the earlier detection results indicate that there has not been a significant collapse in the roof area, suggesting that the roof of the two-step void is manageable.

4. Numerical Simulation Study of the Structural Layout Method for Stepwise Extraction of Working Faces

4.1. Simulation Result Analysis of the One-Step High-Profile Working Face Extraction Process

This simulation takes the 60-10# working face as an example to analyze the stepwise extraction process. Due to the uniform structure of the working faces in the Dongguashan

mining area, the results of the 60-10# working face simulation can also be applied to optimize the extraction sequence of other one-step working faces. The numerical simulation results are analyzed through sectional views along the direction of the working face, with a total of 10 extraction cycles carried out sequentially. The extraction results are shown in Figures 9 and 10.

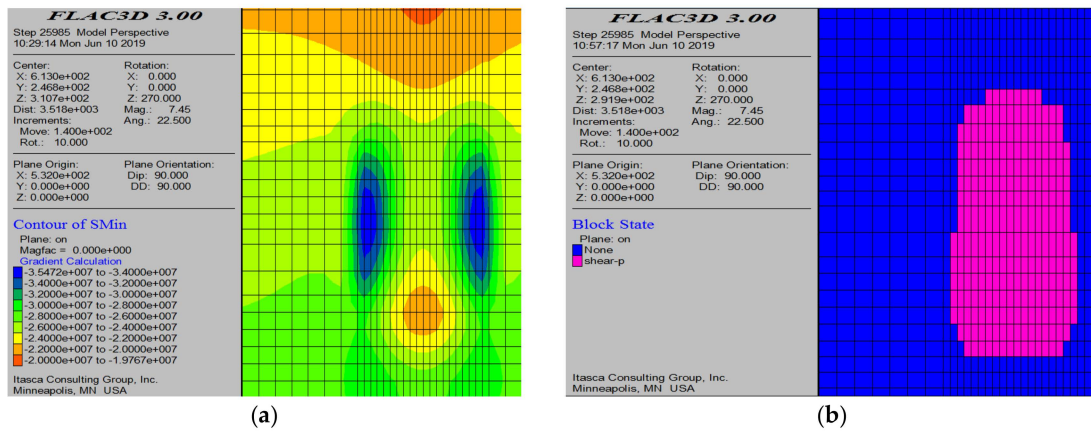


Figure 9. Simulation results before the extraction of the 60-10# working face. (a) Minimum principal stress cloud map; and (b) plastic zone cloud map.

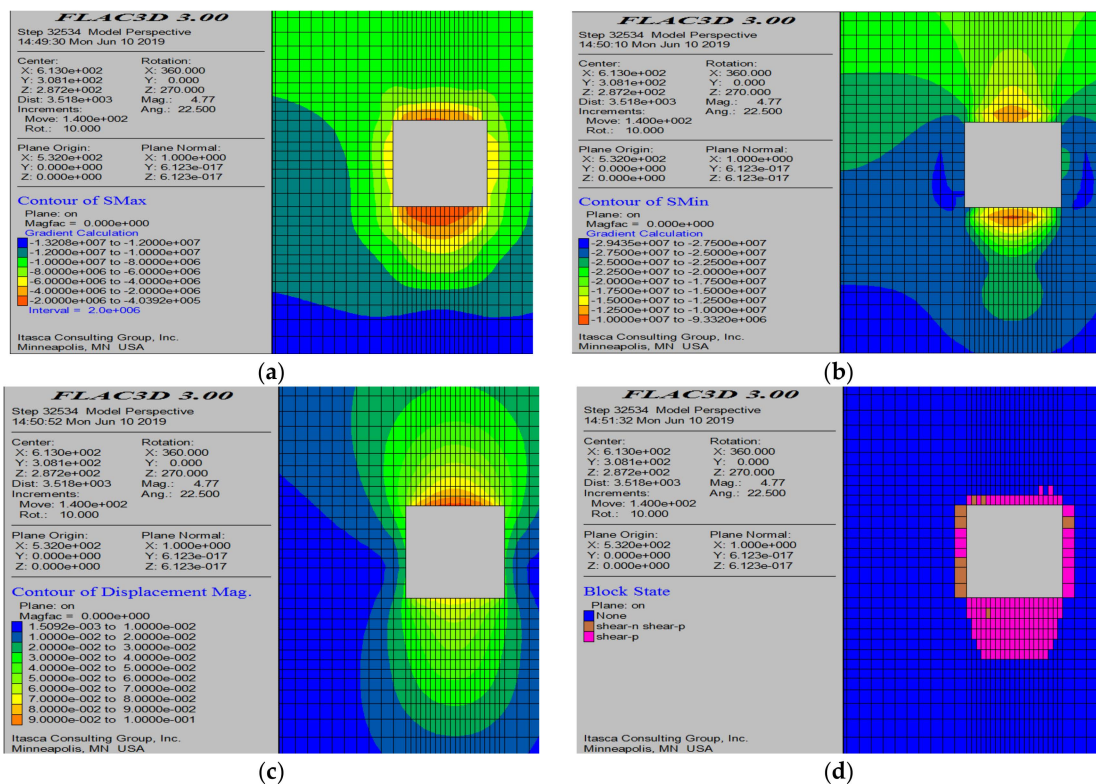


Figure 10. Numerical simulation results after the completion of all mining operations. (a) Maximum principal stress contour map; (b) minimum principal stress contour map; (c) displacement cloud diagram; and (d) plastic zone distribution.

Figure 9 shows the compressive stress cloud diagram and the plastic deformation cloud diagram before mining. From the figure, it can be observed that there are large compressive stress areas at both ends of the 60-10# mining area, with a maximum compressive stress of 35.5 MPa, indicating that the mining area is in a shear state. Through Figures 9 and 10, it

can be seen that the empty area is not subjected to tensile stress; however, after the first end of the mining area is excavated, the maximum compressive stress at the excavation site is released, while the compressive stress at the other end of the mining area continues to increase. The maximum displacement is mainly located at the top of the empty area, and the maximum displacement value is also continuously increasing. The distribution of the plastic zone in the empty area changes from shear-past at the initial excavation to shear-past and shear-now after excavation, indicating that the empty area has previously reached the yield surface but later returned to an elastic state, with some elements also in a shear state. During the continuous excavation process, the main changes are in the maximum compressive stress and maximum displacement values.

We calculated the maximum compressive stress and maximum displacement trend during the stepwise mining process. It can be seen that, during the initial mining process, the maximum compressive stress gradually increases, peaking after the eighth step of mining, reaching a maximum of 39.1 MPa. By the ninth step of mining in the 60-10# panel, the total thickness of the mined area reaches 72 m. In the final two steps of mining, the maximum compressive stress decreases rapidly, indicating some release of stress. From the displacement curve, it is observed that the displacement is relatively large in the early stages of mining, but the trend of increasing displacement slows down during the stepwise mining process, eventually stabilizing, without any sudden changes in displacement.

Overall, using this mining method may lead to a continuous increase in the maximum compressive stress on the other side of the mining area, potentially causing crushing damage to the surrounding rock in the mining chamber. The 60-6# and 60-10# panels at Dongguashan have already suffered significant damage, and adopting this approach may exacerbate the destruction of the surrounding rock in the mining chamber.

From Figures 11 and 12, it can be seen that the maximum principal stress cloud map indicates that, as mining progresses gradually, the surrounding area of the mined-out section is not subjected to tensile stress. In the early stages of mining, the maximum compressive stress is mainly concentrated within the mining area, distributed near both sides of the mined-out section, as shown in Figure 11b. As mining continues, the compressive stress tends to concentrate toward the center of the mining area; however, there is no significant increase in the maximum compressive stress, which stabilizes around 29.4 MPa. From the displacement cloud map, it is evident that the displacement increases with the widening of the mined area, and the maximum displacement continues to rise. The distribution of the plastic zone shows that there are no significant changes surrounding the mined-out area.

In this scheme, the mined-out area is not subjected to tensile stress but is primarily affected by compressive stress. The maximum compressive stress is concentrated in the middle part of the mining area, showing a gradually decreasing trend, indicating that the stress in the mining area is being continuously released. Even after mining to the point where an 8 m thick pillar remains, there is no significant change in the maximum compressive stress. Regarding the displacement of the pillar, as shown in Figure 13, the maximum displacement of the 8 m thick pillar is only 0.84 cm, which is very small.

Based on the changes in the maximum compressive stress and the displacement of the pillar in this scheme, the 8 m thick pillar remains in a relatively stable state. However, considering the reasons such as rock fragmentation and the development of joint fissures north of line 60, it is recommended that the thickness of the pillar left for safe extraction be between 14 and 18 m, with the final extraction conducted in one go. Since the blasting charge for each operation in Dongguashan is below 5 tons and the thickness of each blast is limited, achieving a single extraction of a 14–18 m thickness is difficult due to the large height of the mining area north of line 60. Therefore, this scheme is not recommended.

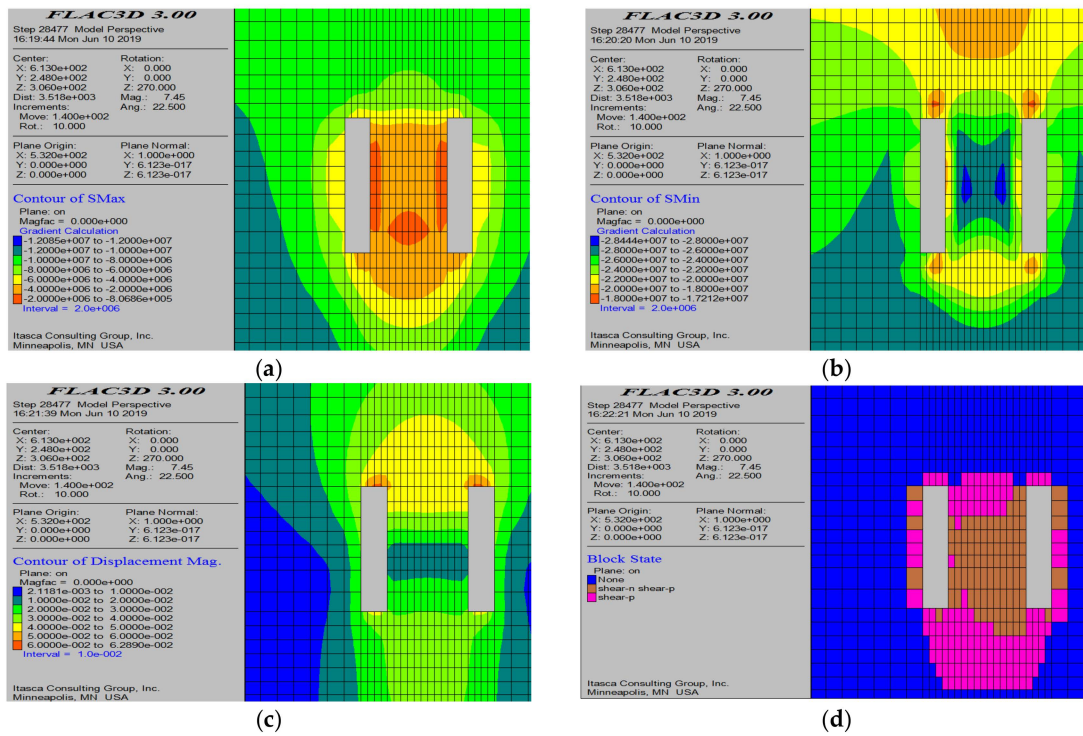


Figure 11. Simulation results after four steps of mining. (a) Maximum principal stress cloud map; (b) minimum principal stress cloud map; (c) displacement cloud map; and (d) plastic zone distribution.

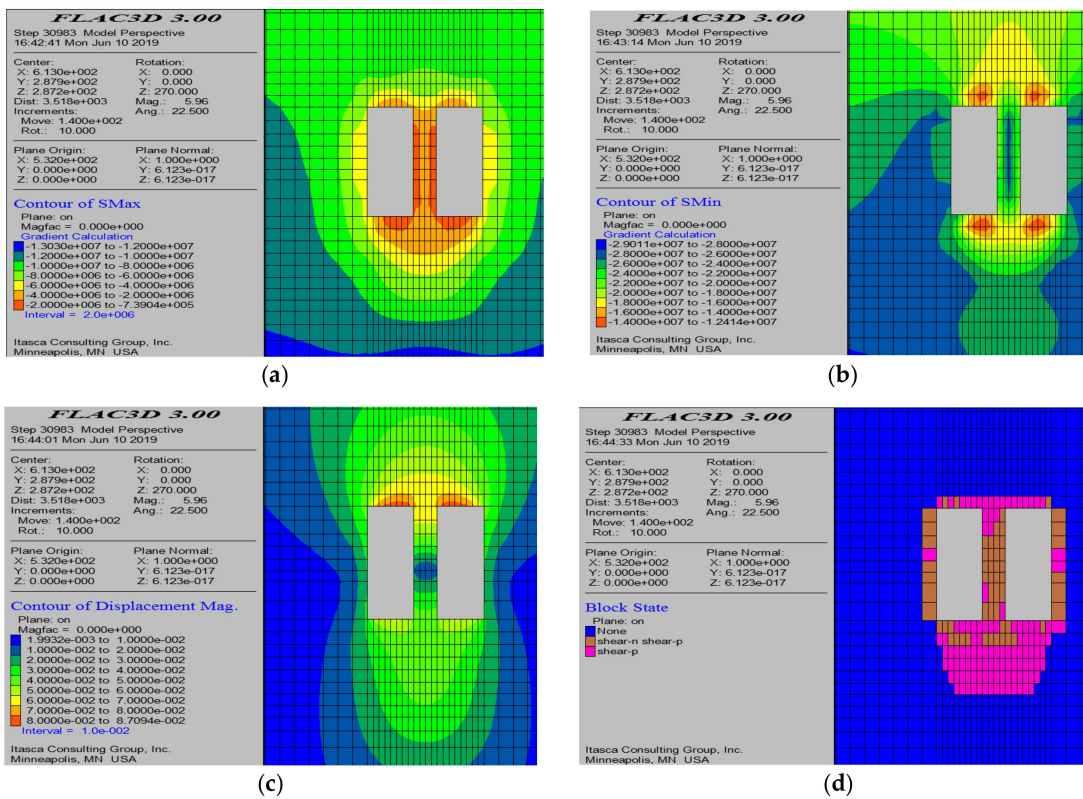


Figure 12. Simulation results after eight steps of mining. (a) Maximum principal stress cloud map; (b) minimum principal stress cloud map; (c) displacement cloud map; and (d) plastic zone distribution.

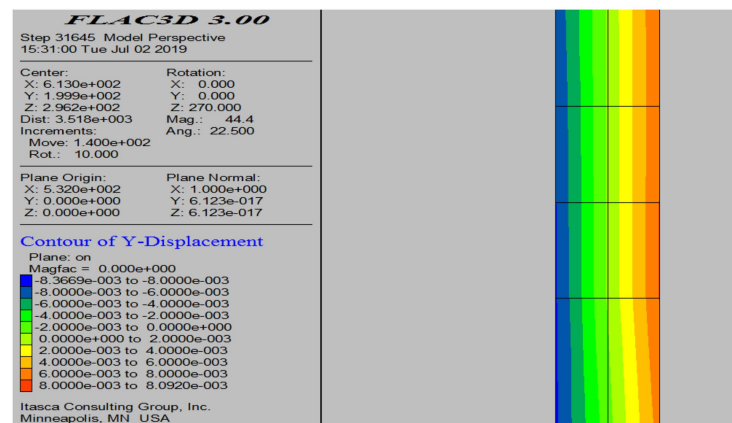


Figure 13. Displacement cloud map of the 8 m thick pillar.

From Figure 14, it can be seen that the maximum principal stress cloud (Figure 14a) and the minimum principal stress cloud (Figure 14b) show that, after mining half of the stope, there is basically no tensile stress acting on the area surrounding the empty space, while the unmined material on the other side of the empty space is subjected to significant compressive stress, with a maximum compressive stress of 37.3 MPa. Before mining, the maximum compressive stress is mainly concentrated on both sides of the stope. After adopting this mining scheme, the maximum compressive stress increases. From the displacement of the roof of the empty space (Figure 14c) and the displacement of the pillars on both sides of the empty space (Figure 14d), it can be observed that the maximum displacement of the roof of the empty space is 8.83 cm, while the lateral displacement of the pillar next to the empty space is 3 cm, which is much smaller than the displacement of the roof of the empty space. Compared to the normal stope displacement, the displacement values are all within a reasonable range.

After the filling of the empty space, as shown in Figure 15, some regions of the filling body exhibit tensile stress, but both the maximum tensile stress value and its range are relatively small. The maximum compressive stress remains at 37.3 MPa, consistent with the maximum compressive stress before filling, indicating that the filling body does not effectively transmit compressive stress. The maximum displacement of the roof after filling is 8.86 cm, which is nearly the same as the displacement after filling. The maximum displacement of the pillars on both sides of the filling body is 2.5 cm, a reduction of 0.5 cm compared to before filling.

From Figure 16, after half of the stope is filled, mining is conducted on the other half of the stope. The results show that there is no tensile stress acting on the empty space, and the maximum compressive stress around the empty space decreases to 30 MPa. The roof displacement of the empty space is 10.4 cm, with the maximum displacement of the filling body in the empty space being 2 cm, and the maximum displacement of the rock mass being 3 cm. Compared to full mining (10 cm), there is not a significant change in the roof displacement of the empty space.

From the above analysis, it can be concluded that, after recovering half of the mining area, the surrounding rock in the empty area is not affected by tensile stress, and the displacement on both sides of the empty area is small, indicating good stability. After filling and recovering the other half of the mining area, the displacement of the roof, the rock on both sides, and the filling body are all within a reasonable range, and the maximum compressive stress decreased. In summary, this method has been proven feasible through a numerical simulation; however, the process on-site is complex and the pressure on mining production tasks is significant, so it cannot be widely promoted, although it may be considered for application in certain mining areas.

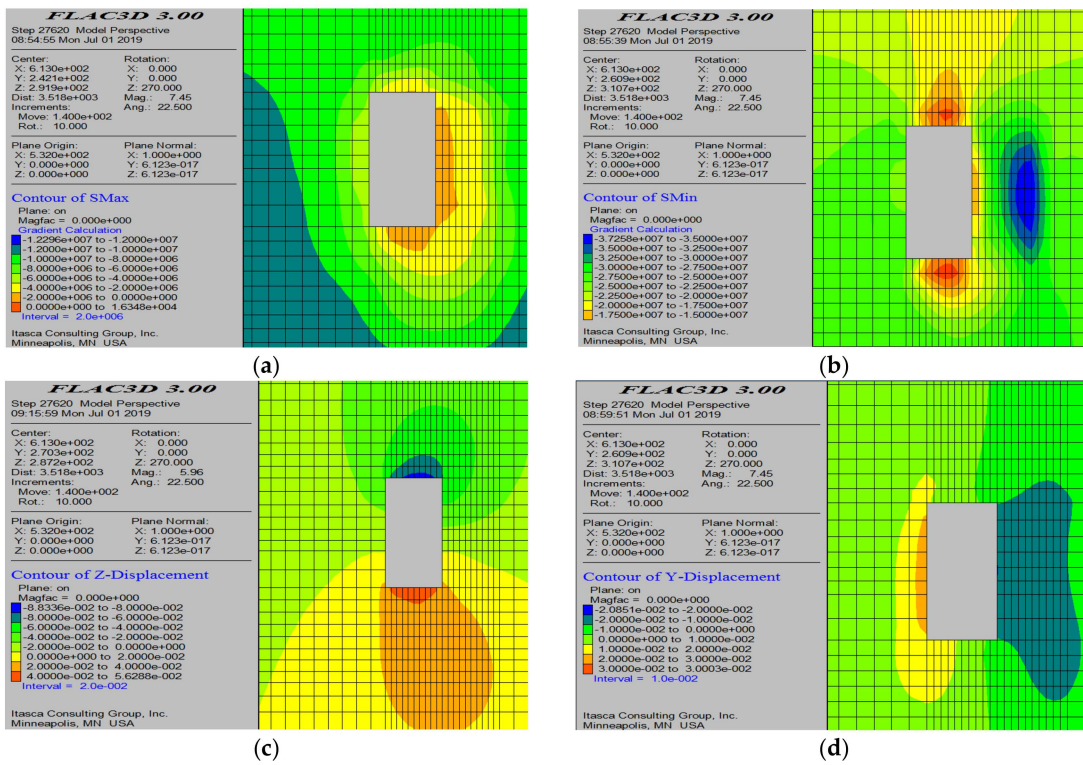


Figure 14. Simulation results after half of the extraction. (a) Maximum principal stress cloud map; (b) minimum principal stress cloud map; (c) displacement cloud map of the roof; and (d) displacement cloud map of the pillars.

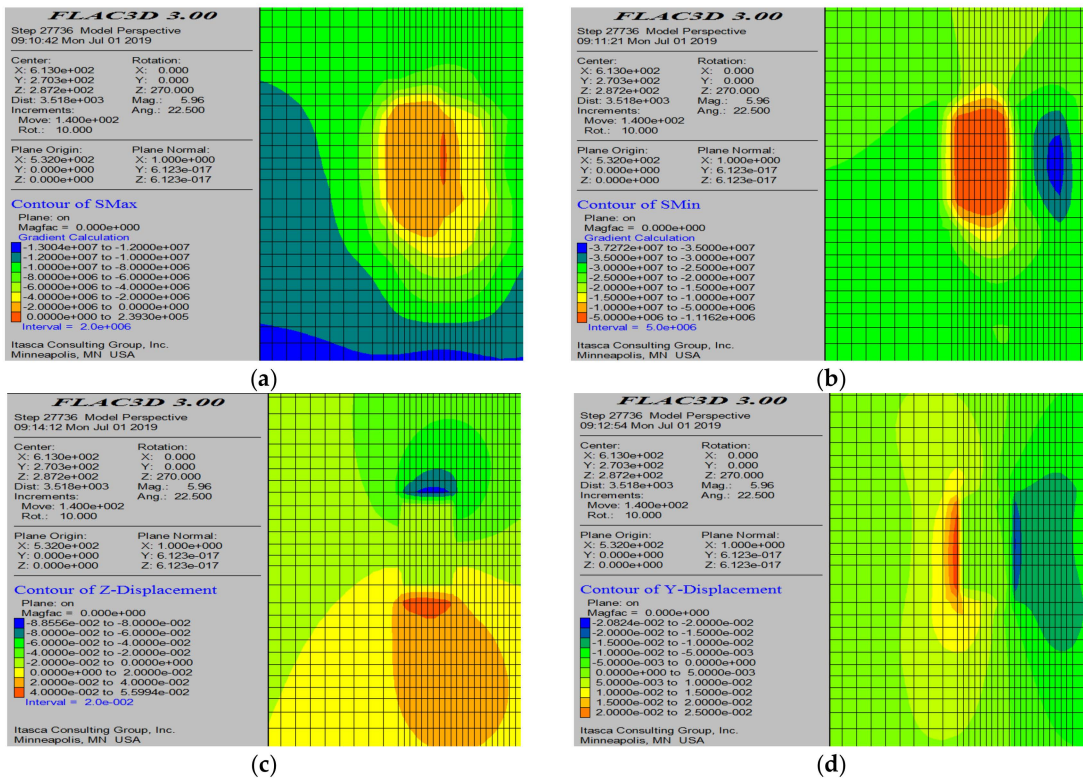


Figure 15. Simulation results after half of the filling. (a) Maximum principal stress cloud map; (b) minimum principal stress cloud map; (c) displacement cloud map of the roof; and (d) displacement cloud map of the pillars.

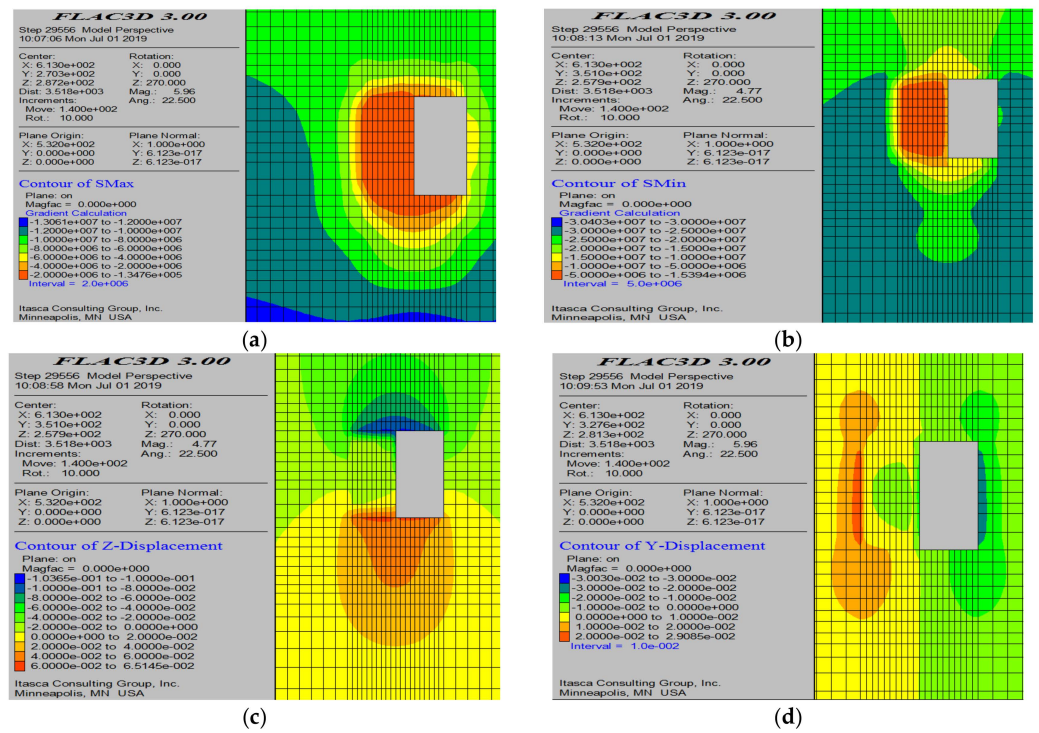


Figure 16. Simulation results after the recovery of the other half. (a) Maximum principal stress cloud map; (b) minimum principal stress cloud map; (c) displacement cloud map of the roof; and (d) displacement cloud map of the pillars.

From the previous simulation results, it is known that, after the two-step mining, the filling body is relatively stable, and the stability of the filling body is an important foundation for this plan. After reducing the dimensions in the middle of the one-step mining area, the thickness of the filling body in the central area of the one-step mining needs further numerical simulation calculations to determine whether it can meet the stability requirements. Due to the change in the mining area dimensions, this numerical simulation requires redesigning and recalculating for the model, as shown in Figure 17. This simulation takes the 62 line mining area as a reference and focuses on the concentrated high mining areas for the numerical simulation calculations, covering the range from the 62-1# to the 62-12# mining areas. The height of the model from the 60-4# to the 60-12# mining areas is set at 125 m.

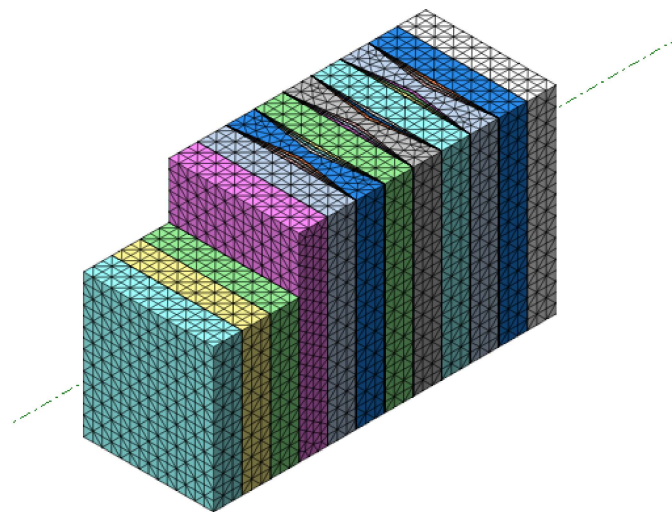


Figure 17. Model of the 62-2# to 62-12# mining areas.

- (1) Determine the thickness of the retained rock mass on both sides of the middle section of the mining area.

In this scheme, a certain thickness of rock mass is retained on both sides of the middle section of the one-step mining area for the two-step mining. The thickness of the retained rock mass needs to be confirmed through simulation calculations. This simulation involves a numerical analysis of the triangular rock columns with thicknesses of 2 m, 4 m, and 6 m retained on both sides of the mining area. The simulation results are as follows.

Figure 18 presents the simulation results of a single void after complete extraction using the original mining method, compared with the new scheme. The results show that the maximum tensile stress on both sides of the void is 1.42 MPa, with a small range, which may lead to localized spalling; the maximum compressive stress is concentrated at the four corners of the void, reaching 40.9 MPa. The maximum displacement of the roof is 6.04 cm, while the displacement of the surrounding rock is 5.8 cm.

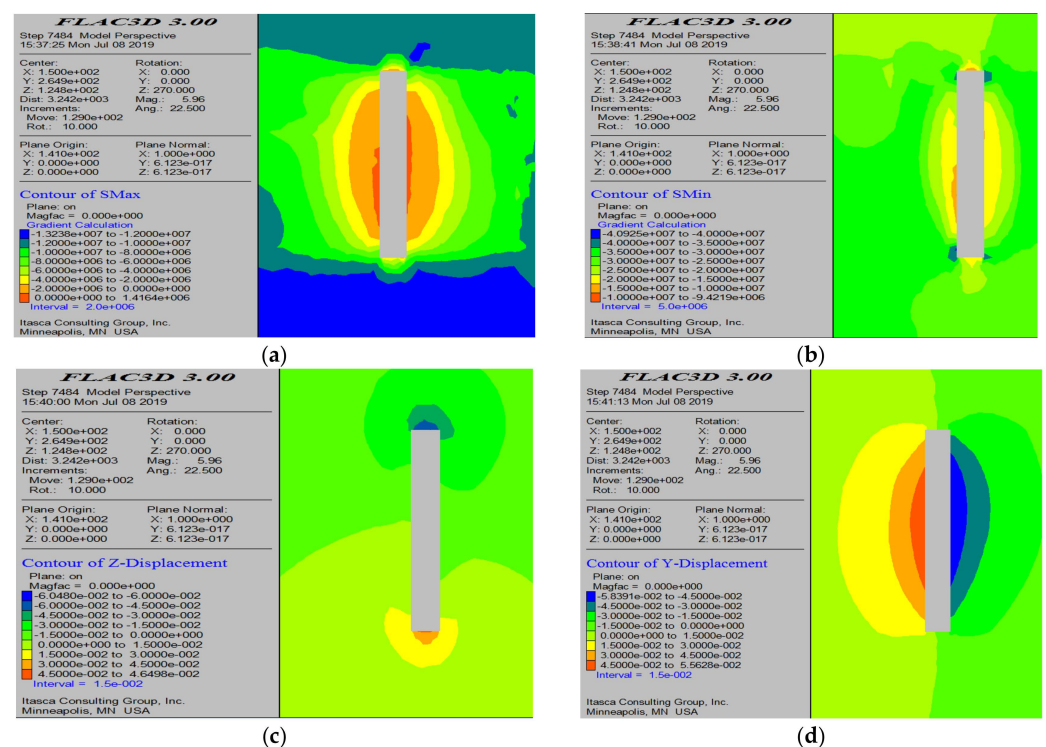


Figure 18. Simulation results after the mining area is extracted according to the original mining method. (a) Maximum principal stress cloud map; (b) minimum principal stress cloud map; (c) displacement cloud map of the roof; and (d) displacement cloud map of the pillars.

Figure 19 shows the simulation results with 2 m thick pillars left on both sides of the mining area. At this point, the maximum tensile stress on both sides of the void decreases to 1.03 MPa, but the maximum compressive stress increases to 51.9 MPa. The maximum displacement of the roof is 5.0 cm, and the displacement of the surrounding rock increases to 6 cm. Compared to the original mining method, while leaving the pillars reduces tensile stress, it increases displacement and compressive stress, which is not conducive to the stability of the void.

Figure 20 shows the simulation results with a 4 m thick pillar left on both sides of the mining site. The results indicate that the maximum tensile stress on both sides of the empty area is 1.03 MPa, which is a decrease; the maximum compressive stress is concentrated on the top and bottom plates, reaching 61.51 MPa, with a small range. The maximum displacement of the top plate decreased to 3.96 cm, and the displacement of the surrounding rock significantly reduced, forming two regions with a maximum displacement of only

1.14 cm, which is a substantial decrease compared to 5.8 cm from the original mining method, indicating a significant improvement in the stability of the pillars.

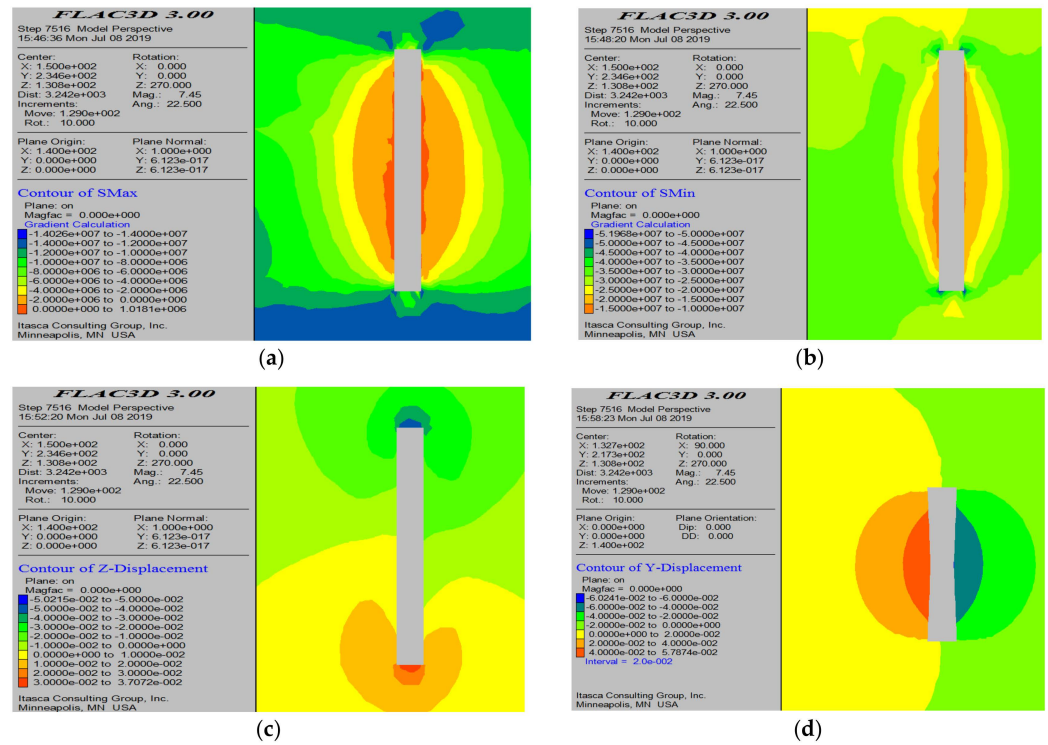


Figure 19. Simulation results with 2m thick pillars left on both sides of the mining area. (a) Maximum principal stress cloud map; (b) minimum principal stress cloud map; (c) displacement cloud map of the roof; and (d) displacement cloud map of the pillars.

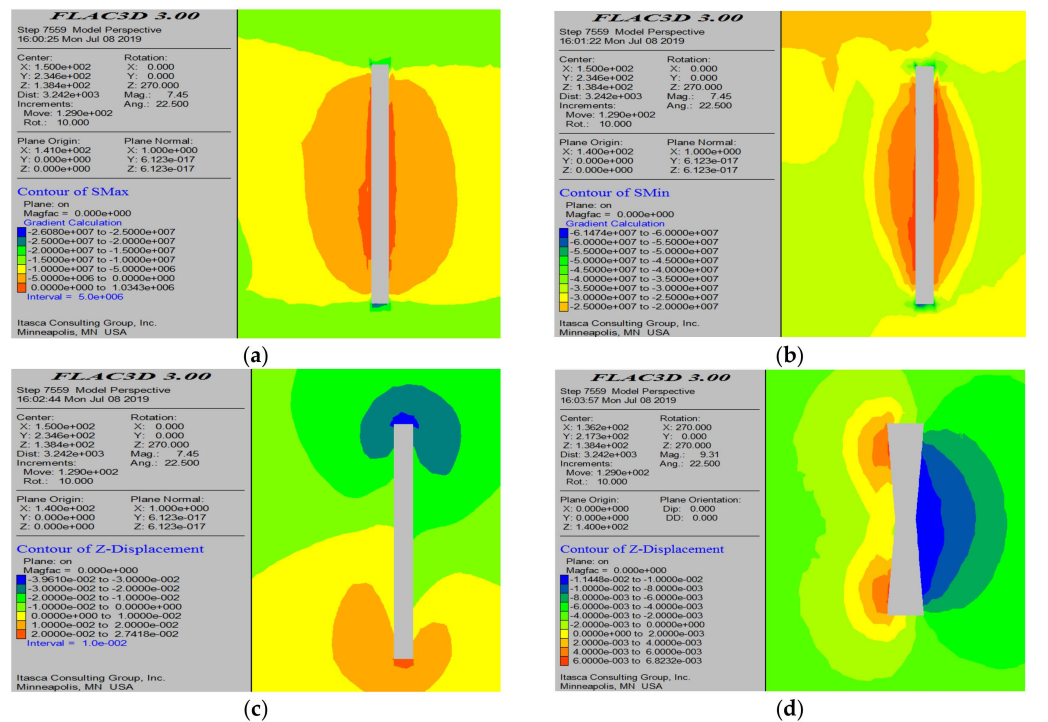


Figure 20. Simulation results with 4 m thick pillars left on both sides of the mining area. (a) Maximum principal stress cloud map; (b) minimum principal stress cloud map; (c) displacement cloud map of the roof; and (d) displacement cloud map of the pillars.

Figure 21 shows the simulation results with a 6 m thick pillar left on both sides. The results indicate that the maximum tensile stress is 1.46 MPa, which is similar to that of the original mining method, but the range of tensile stress has increased. The maximum compressive stress is mainly located on the top and bottom plates, reaching 49.9 MPa, which is lower than in the previous two scenarios. The maximum displacement of the top plate is 3.2 cm, and the displacement of the surrounding rock on both sides has returned to a single region with a maximum displacement of 6.1 cm, indicating that the apex area is prone to collapse.

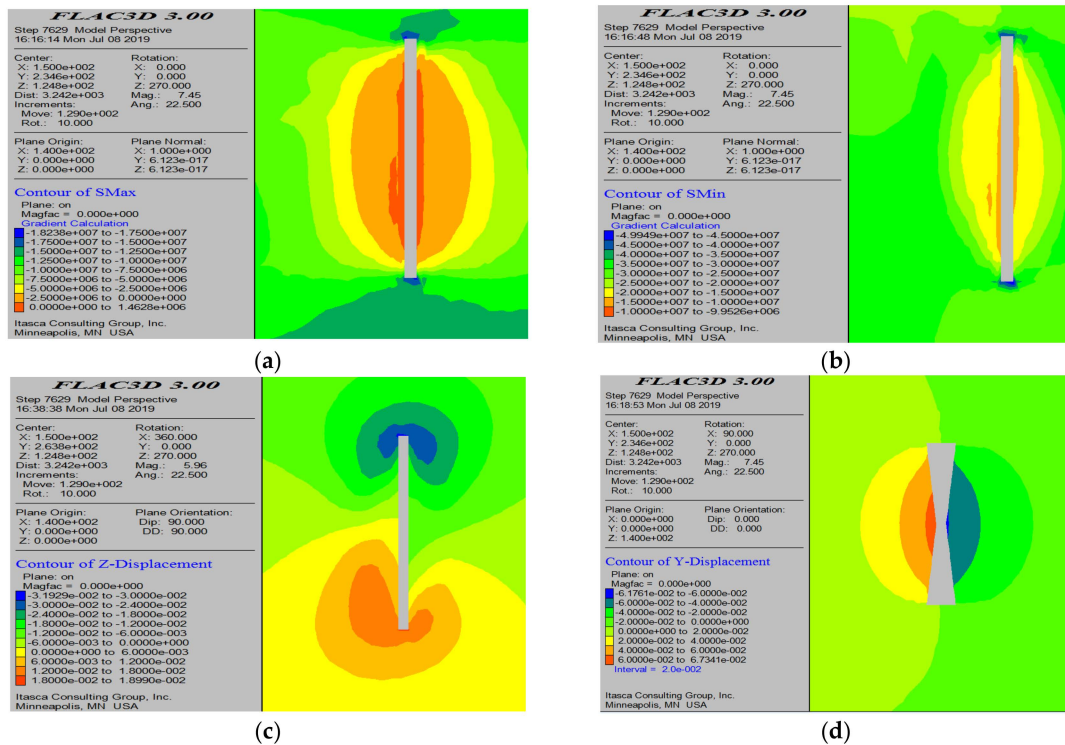


Figure 21. Simulation results with a 6 m thick pillar left on one side of the central area of the mining site. (a) Maximum principal stress cloud map; (b) minimum principal stress cloud map; (c) displacement cloud map of the roof; and (d) displacement cloud map of the pillars.

In summary, leaving a 4 m thick triangular pillar on both sides of the mining site as part of the two-step mining scheme can significantly reduce the displacement of the surrounding rock in the empty area, and the displacement of the top plate is also reduced. Although the maximum compressive stress of this scheme is relatively high, its impact range is small, so a pillar thickness of 4 m is recommended.

(2) Simulation Results after Applying This Scheme to Adjacent One-Step High Mining Sites

As the dimensions of the middle section of the one-step mining site are reduced, the extraction range of the two-step mining site will increase, leading to a larger exposed area of the empty zone. If this scheme is applied to adjacent one-step mining sites, the exposed area of the top plate of the two-step empty zone will increase, and the thickness of the fill on both sides of the empty zone will decrease, which necessitates further verification of the stability of the empty zone. Therefore, this study compares and analyzes the changes in stress and displacement after the extraction of the 60-7# two-step mining site following the reduction of the middle section dimensions in the 60-6# and 60-8# mining sites. The simulation results are as follows:

Figure 22 shows the simulation results after completing the two-step mining according to the original mining method, mainly for comparison with this scheme. From the simulation results, it can be seen that only a small portion of the fill material on both sides of the

void is affected by tensile stress after mining, with a maximum tensile stress of 1.47 MPa, which may lead to some falling of the fill material. From the minimum principal stress cloud map (Figure 22b), it can be observed that there is no stress concentration around the void, and the maximum compressive stress is located in the surrounding areas of the one-step and two-step mining after extraction, which has little impact on the void. The maximum displacement of the roof is 13.6 cm, while the maximum displacement of the fill material on both sides of the void is 5.2 cm.

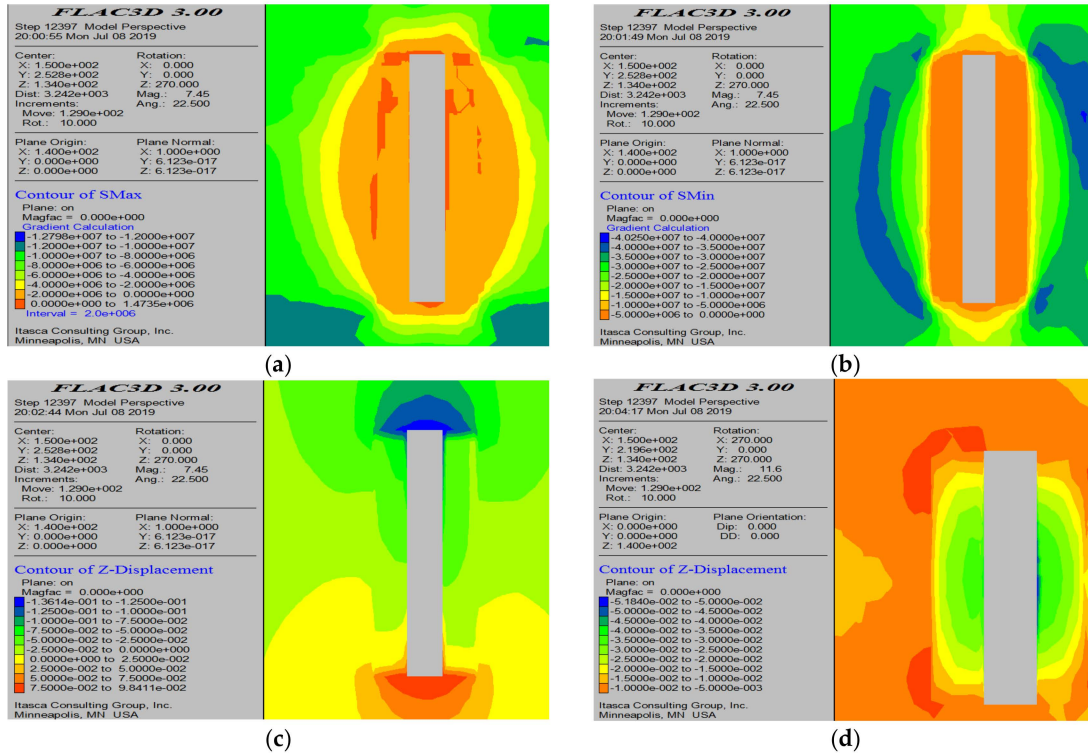


Figure 22. Simulation calculation results of the original two-step mining method. (a) Maximum principal stress cloud map; (b) minimum principal stress cloud map; (c) displacement cloud map of the roof; and (d) displacement cloud map of the pillars.

After adopting the scheme of leaving a 4 m thick pillar in the middle of the mining area, the two-step mining area is enlarged, increasing the exposed area of the void, and the simulation results are shown in Figure 23. From the maximum principal stress cloud map (Figure 23a), it can be seen that only a small portion of the fill material is subjected to tensile stress, with a maximum tensile stress of 0.45 MPa. The maximum compressive stress is located around the one-step mining area, and the stress in the two-step mining area is basically released. The displacement of the void roof is 12.8 cm, and the displacement of the fill material on both sides of the void is 7.2 cm, but the range is very small, with the general displacement of the fill material being between 2 and 4 cm, which is sufficient to maintain the stability of the fill material. When continuously applying this scheme for extraction in the one-step mining area, compared to the original mining scheme, the tensile stress is reduced, the roof displacement is lowered, and there are no significant changes in the displacement of the fill material, with the only noticeable changes being in the range and magnitude of the maximum compressive stress. Therefore, it is feasible to continue to apply this scheme in the one-step mining area.

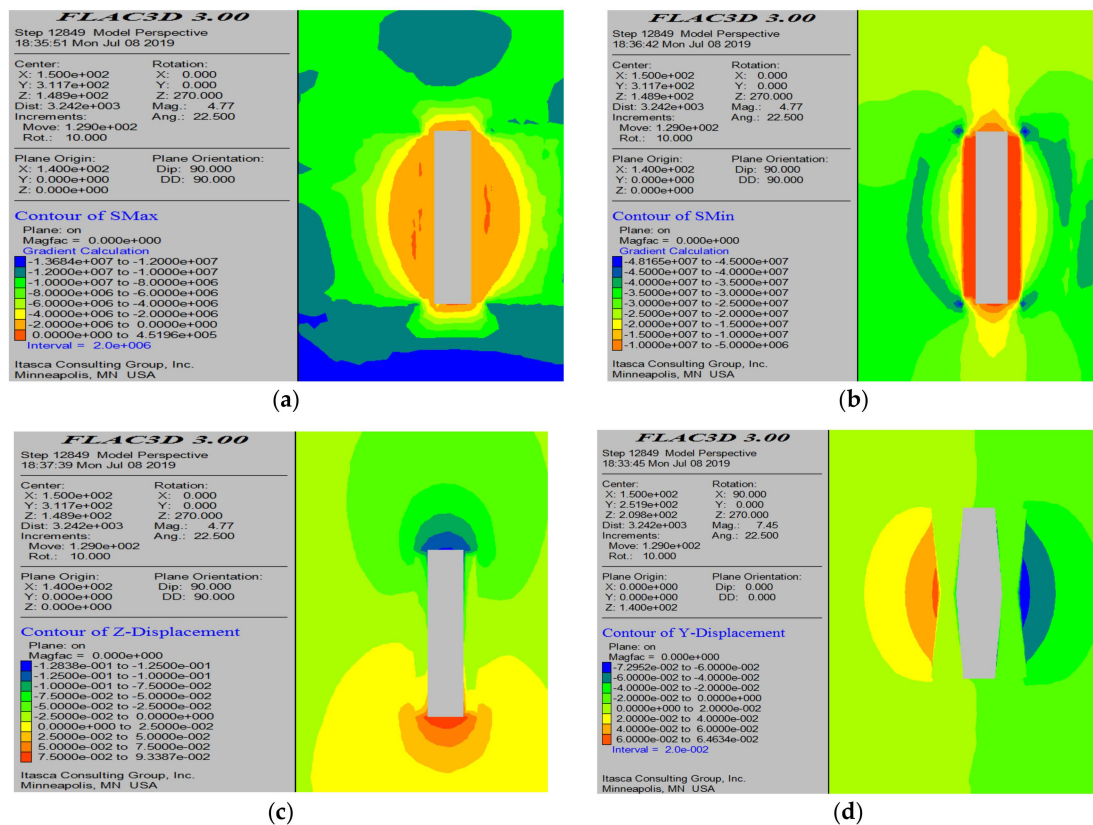


Figure 23. Simulation calculation results of the two-step mining after applying this scheme. (a) Maximum principal stress cloud map; (b) minimum principal stress cloud map; (c) displacement cloud map of the roof; and (d) displacement cloud map of the pillars.

In summary, gradually mining from one side of the working area to the other can lead to stress concentration at the opposite end, exacerbating damage to the chamber and rendering it unsuitable for all mining areas. In the mining areas north of line 60 at Dongguashan, after adopting this mining sequence, some fragmented regions or large mining areas experience severe damage in the void after extraction. Using the method of mining from both sides toward the center, the maximum compressive stress gradually decreases, and the stress concentration is released during the initial extraction, which is beneficial for enhancing the stability of the chamber. However, this scheme requires retaining a 14–18 m thick pillar in the middle of the working area. Due to blasting restrictions and rock fragmentation, it is challenging to blast the pillar all at once, making it prone to collapse and affecting safe operations; therefore, it is not recommended. The “mining-filling-mining” scheme can reduce the deformation of the roof and surrounding rock, but it involves significant closure work, a complex filling process, and high organizational difficulties in production, which reduces the production capacity of the working area and impacts the completion of mining tasks. Hence, it is only suitable for localized applications and not recommended for widespread promotion.

The plan to reduce the width of the one-step mining area, by dividing a larger exposed surface into two surfaces to form triangular pillars, enhances the strength of the pillars. The simulation results show that the displacement of the rock on both sides of the void is significantly reduced, effectively protecting the pillars in the two-step mining area. Even if the rock on both sides has developed joints and fractures, the scheme retains a certain thickness of rock, providing adequate protection. When continuously applying this scheme in adjacent one-step mining areas, although the exposed area of the two-step void increases, there are no significant changes in the displacement of the fill material, roof displacement, or tensile stress variation compared to the original scheme. Although the compressive

stress increases, its range is small and has little impact. Therefore, it is recommended to actively adopt this scheme for the extraction of large one-step mining areas.

4.2. Analysis of the Simulation Results of the Two-Step High Mining Area Extraction Process

During the recovery process in the two-step mining area, significant changes occur in the surrounding rock mass, transforming from high-strength ore rock to lower strength fill material. Additionally, during the recovery process, stress is further released, and the areas where stress is concentrated shift significantly. Therefore, the analysis of the two-step mining area focuses on the following two aspects: first, examining the changes in the maximum compressive stress through cross-sectional diagrams along the mining area, where the patterns of changes in the maximum stress position can be easily identified; second, observing the displacement changes of the fill material on both sides of the void from a direction perpendicular to the mining area. This numerical simulation uses the 60-23# mining area as a case study to conduct numerical calculations on the recovery sequence.

From the minimum principal stress cloud map before the recovery of the 60-23# mining area, it can be seen that the maximum compressive stress has shifted to the bottom area of the mining area where it intersects with the cross-cut passage. The compressive stress values within the mining area are relatively low, ranging from 25 MPa to 30 MPa. The maximum principal stress cloud map indicates that, after the initial excavation of the mining area, the internal rock mass is subjected to tensile stress, which is relatively small, and the range of tensile stress is also limited, essentially being insufficient to damage the rock mass. The minimum principal stress cloud map shows that, during the recovery process from one end of the mining area to the other, the bottom of the unmined end of the mining area experiences significant compressive stress, and, as recovery continues, the maximum compressive stress keeps changing.

From Figures 24 and 25, the maximum principal stress cloud diagram indicates that, during the process of mining from the center towards both sides, both sides of the empty area experience tensile stress within a certain range. However, the tensile stress is relatively small, and its range is limited. As the mining progresses, the position of the tensile stress gradually changes, and, upon nearing the completion of the mining, the roof of the empty area experiences some tensile stress, albeit at a low level. The minimum principal stress cloud diagram shows that the maximum compressive stress is primarily located at the bottom of both sides of the mining area and at the intersection with the cross-cut tunnel. The maximum compressive stress also varies continuously as the mining advances.

From Figure 26, it can be seen that, after half of the mining in the area is completed, the tensile stress is very low, only 0.21 MPa. The maximum compressive stress is located at the junction of the unmined area and the cross-cut passage, reaching 36.4 MPa, but the range is not large. The maximum displacement of the roof in the void is 12.6 cm, while the maximum displacement of the filling material on both sides of the void is 4 cm.

From Figure 27, it can be observed that, after the mining area is mined and backfilled and additional mining is conducted, the area surrounding the void is basically not subjected to tensile stress. The maximum compressive stress around the void decreases, with the maximum displacement of the roof reaching 14.1 cm and the displacement of the filling material on both sides being 2 m.

In the original mining method, the void is essentially not subjected to tensile stress, and the maximum compressive stress decreases, with the maximum displacement of the roof being 14.2 cm and the maximum displacement of the filling material being 2 cm. Compared to this method, there is no significant difference. From the above analysis, it can be concluded that the simulation calculation based on the filling scheme shows no significant differences when compared to the original mining plan for the two-step method. Additionally, this scheme requires two rounds of backfilling, which increases the amount of sealing work and complicates the backfilling process. Therefore, it is not recommended for widespread adoption.

Based on the above extraction schemes, when adopting the approach of gradually mining from the middle to both sides, the initial displacement of the roof and filling body is relatively large, making the central area of the void prone to collapse; therefore, this scheme is not recommended. Although the “Mining-Filling-Mining” scheme does not transfer stress to the filling body, it can effectively reduce the deformation of the roof and filling body. Thus, from the perspective of protecting the void, it has a positive effect. However, this scheme involves two filling processes, complicating the filling operation, increasing the closure workload, and making the production organization more challenging. Therefore, the “Mining-Filling-Mining” scheme is not recommended for widespread application, but could be considered for some very tall mining areas. Combining the analysis of the numerical simulation results, after the completion of the first-step mining, the stress has been released. Based on the numerical simulation results of various schemes for the second-step mining, it is recommended to adopt the scheme of gradually mining from one side of the mining area to the other (the original mining sequence) for the second-step mining.

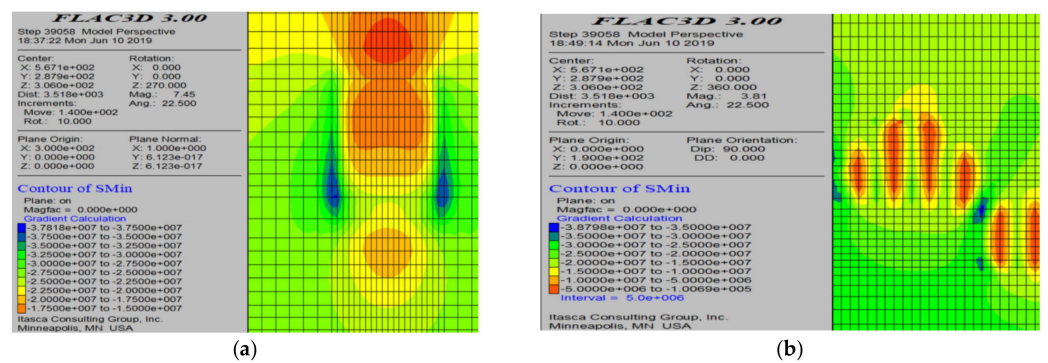


Figure 24. Minimum principal stress cloud diagram before the mining of the 60-23# mining area. (a) Profile cloud diagram along the mining area direction; and (b) profile cloud diagram perpendicular to the mining area direction.

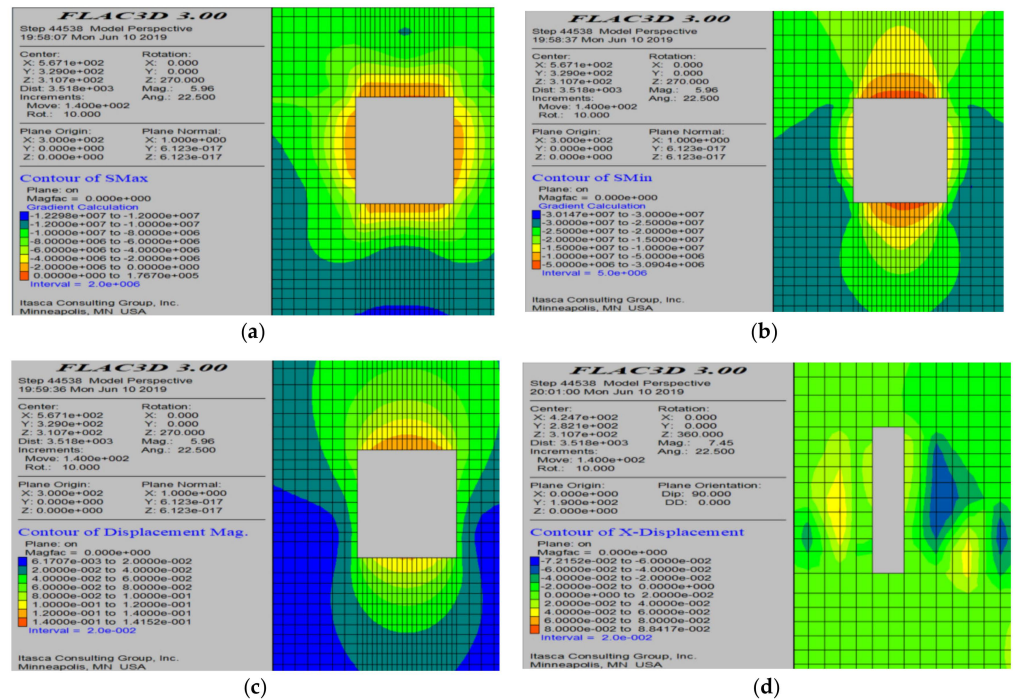


Figure 25. Simulation calculation results after mining completion. (a) Maximum principal stress cloud map; (b) minimum principal stress cloud map; (c) profile cloud diagram along the mining area direction; and (d) profile cloud diagram perpendicular to the mining area direction.

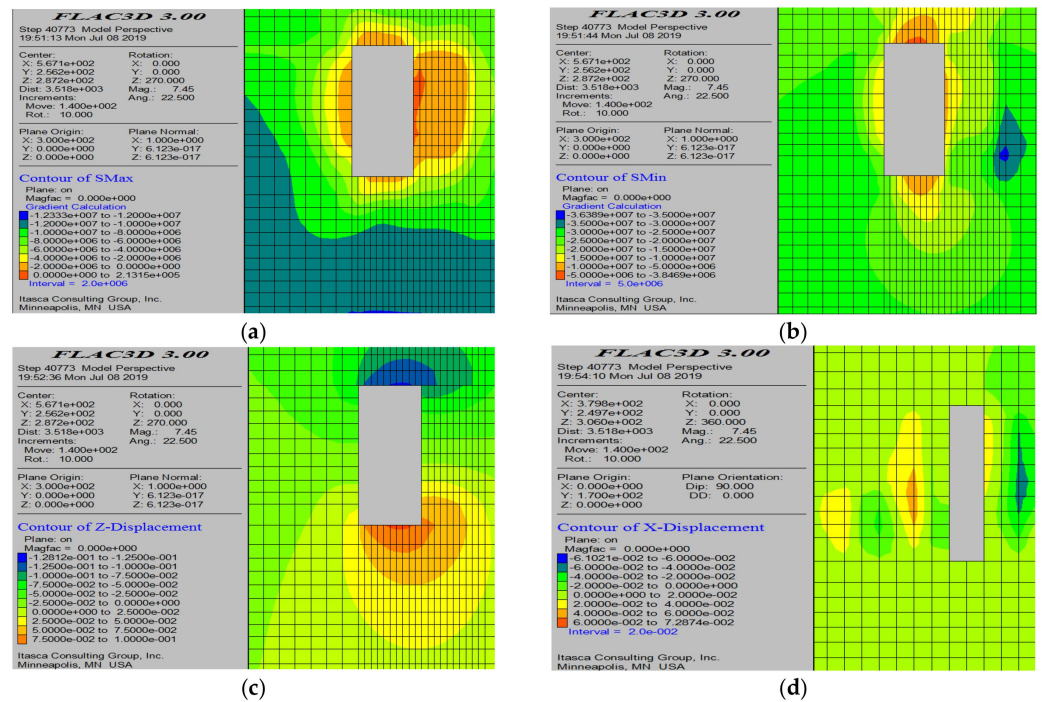


Figure 26. Numerical simulation results of slope 23# stope with first half stope. (a) Maximum principal stress cloud map; (b) minimum principal stress cloud map; (c) profile cloud diagram along the mining area direction; and (d) profile cloud diagram perpendicular to the mining area direction.

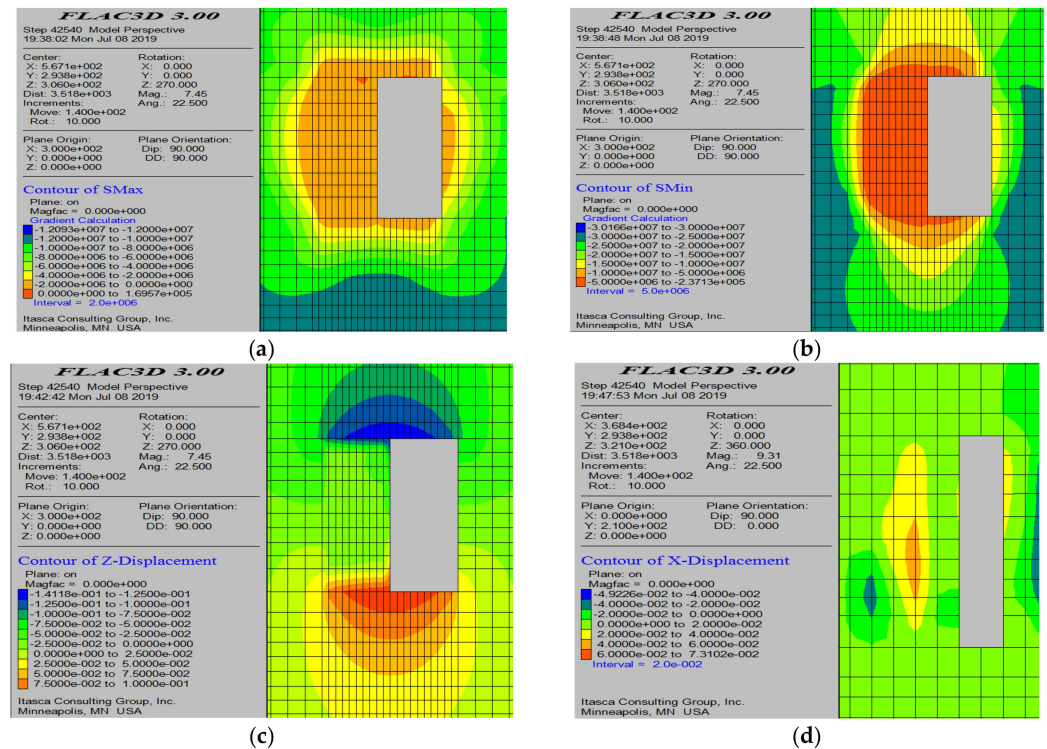


Figure 27. Numerical simulation results after the second half of the 23# mining area is extracted. (a) Maximum principal stress cloud map; (b) minimum principal stress cloud map; (c) profile cloud diagram along the mining area direction; and (d) profile cloud diagram perpendicular to the mining area direction.

5. Conclusions

This study focuses on the large mining areas of the Dongguashan copper deposit, using the geological conditions and mechanical parameters of the ore body as a basis. A three-dimensional model of the mining area was established using FLAC3D numerical simulation software, and a detailed analysis of the stress distribution and displacement changes under different mining schemes was conducted. The following conclusions were drawn:

- (1) **Stress conditions:** The filling body can improve the distribution of stress to some extent; however, it cannot alter the overall trend of stress transfer. The filling body itself cannot bear most of the transferred stress, which remains supported by the surrounding rock with a higher strength. In the second-step mining area, the adjacent filling body cannot bear the transferred stress, resulting in significantly higher maximum values of tensile, compressive, and shear stresses compared to the first-step mining area.
- (2) **Displacement and plastic zone distribution:** The displacement values and the distribution of plastic zones in the second-step mining area are notably higher than those in the first-step mining area. The displacement distribution of the roof in the second-step mining area shows relatively gentle numerical changes and uniform subsidence. Although there are plastic zones in the roof, they do not penetrate the entire roof. Considering the dynamic load caused by blasting vibrations, it is essential to control the scale of the maximum amount of explosives during blasting in the second-step mining area to minimize the impact of blasting on the mining area and the surrounding filling body.
- (3) **Conventional mining methods are prone to stress concentration in the rock and increased roof displacement, making them unsuitable for large mining areas in complex geological conditions. Various optimized mining schemes were proposed and validated. The scheme of “reducing the intermediate dimensions of the first-step mining area” significantly reduces the displacement of the rock on both sides of the void and alleviates the stress concentration, effectively enhancing the stability of the void. The second-step mining should adopt a gradual approach, progressively mining from one side to the other, to minimize the stress concentration and displacement changes in the mining area and ensure the stability of the void.**

Author Contributions: Conceptualization, Q.Z. and M.H.; methodology, Q.Z.; resources, M.H.; writing—original draft preparation, M.H.; writing—review and editing, Q.Z. and J.G.; visualization, M.H.; and funding acquisition, J.G. All authors have read and agreed to the published version of this manuscript.

Funding: This research was funded by the National Natural Science Foundation of China (no. 52174140).

Institutional Review Board Statement: Not applicable.

Informed Consent Statement: Not applicable.

Data Availability Statement: Data will be made available on request.

Conflicts of Interest: Author Mingjian Huang was employed by the company Hunan Lianshao Construction Engineering (Group) Co., Ltd. The remaining authors declare that the research was conducted in the absence of any commercial or financial relationships that could be construed as a potential conflict of interest.

References

1. Wang, Y.M.; Wu, A.X.; Chen, X.S.; Yang, B.H.; Su, Y.D. New mining technique with big panels and stopes in deep mine. *Trans. Nonferrous Met. Soc. China* **2008**, *18*, 183–189. [[CrossRef](#)]
2. Yu, W.; Zhai, S.; Gao, Q. Stability evaluation indexes of deep stope pillar and roadway surrounding rock. *Disaster Adv.* **2012**, *5*, 120–126.
3. Chen, S.H.; Zhang, Z.H. Determination of coal pillar width and support parameters in deep coal mines—A case study. *J. Test. Eval.* **2018**, *47*, 3160–3173. [[CrossRef](#)]

4. Tuncay, D.; Tulu, I.B.; Klemetti, T. Re-analysis of Abutment Angle Method for Moderate and Deep Cover Retreat Room and Pillar Mines and Investigation of Loading Mechanics Using Finite Volume Modeling. *Rock Mech. Rock Eng.* **2021**, *54*, 3447–3468. [[CrossRef](#)]
5. McColl, S.T. Chapter 2—Landslide causes and triggers. In *Landslide Hazards, Risks, and Disasters*; Hazards and Disasters Series; Elsevier: Amsterdam, The Netherlands, 2022; pp. 13–41.
6. Wei, Z.L.; Lü, Q.; Sun, H.Y.; Shang, Y.Q. Estimating the rainfall threshold of a deep-seated landslide by integrating models for predicting the groundwater level and stability analysis of the slope. *Eng. Geol.* **2019**, *253*, 14–26. [[CrossRef](#)]
7. Mohanto, S.; Debasis, D. Prediction of Plastic Damage Index for Assessing Rib Pillar Stability in Underground Metal Mine Using Multi-Variate Regression and Artificial Neural Network Techniques. *Geotech. Geol. Eng.* **2020**, *38*, 767–790. [[CrossRef](#)]
8. Qi, C.; Fourie, A. Numerical Investigation of the Stress Distribution in Backfilled Stopes Considering Creep Behaviour of Rock Mass. *Rock Mech. Rock Eng.* **2019**, *52*, 3353–3371. [[CrossRef](#)]
9. Wang, Y.; Tang, P.; Han, J.; Li, P. Energy-Driven Fracture and Instability of Deeply Buried Rock under Triaxial Alternative Fatigue Loads and Multistage Unloading Conditions: Prior Fatigue Damage Effect. *Int. J. Fatigue* **2023**, *168*, 107410. [[CrossRef](#)]
10. Guo, Q.; Guo, W.; Yang, W.; Li, L.; Hu, C. Study on Crushed-Stone Cementation Properties and Bottom Stope Stability of Goaf by Open Stope Mining in Inclined Ore Bodies. *Appl. Sci.* **2024**, *14*, 9945. [[CrossRef](#)]
11. Liu, S.; Zhao, J.; Zhao, X. Limit equilibrium method for assessing slope stability of high rockfill dams. *J. Rock Mech. Geotech. Eng.* **2020**, *12*, 451–461.
12. Greif, V.; Vlčko, J. Key Block Theory Application for Rock Slope Stability Analysis in the Foundations of Medieval Castles in Slovakia. *J. Cult. Herit.* **2013**, *14*, 359–364. [[CrossRef](#)]
13. Li, F.; Zhang, T. Fracture mechanics analysis of rock failure in underground mining: Recent advances and future directions. *Int. J. Rock Mech. Min. Sci.* **2020**, *122*, 104259.
14. Ash, N.F. Application of Numerical Simulation Using a Progressive Failure Approach to Underground Coal Mine Stability Analysis. Ph.D. Thesis, The University of Alabama, Tuscaloosa, AL, USA, 1987.
15. Yu, T.; Teng, J.; Wong, Y.; Dong, S. Finite element modeling of confined concrete-II: Plastic-damage model. *Eng. Struct.* **2010**, *32*, 680–691. [[CrossRef](#)]
16. Usto, J.; Castro, J.; Cicero, S. Energy-Based Approach for Fracture Assessment of Several Rocks Containing U-Shaped Notches through the Application of the SED Criterion. *Int. J. Rock Mech. Min. Sci.* **2018**, *110*, 306–315.
17. Su, C.; Zhu, H.; Cai, W.; Wu, W.; Zhang, Q. Elastic Perfect Plastic Rock Mass Analysis and Equivalent GSI Determination Considering Strain-Softening Behavior and Three-Dimensional Strength. *Tunn. Undergr. Space Technol.* **2023**, *142*, 105422. [[CrossRef](#)]
18. Ding, Q.-L.; Peng, Y.-Y.; Cheng, Z.; Wang, P. Numerical Simulation of Slope Stability during Underground Excavation Using the Lagrange Element Strength Reduction Method. *Minerals* **2022**, *12*, 1054. [[CrossRef](#)]
19. Lisjak, A.; Young-Schultz, T.; Li, B.; He, L.; Tatone, B.; Mahabadi, O. A Novel Rockbolt Formulation for a GPU-Accelerated, Finite-Discrete Element Method Code and Its Application to Underground Excavations. *Int. J. Rock Mech. Min. Sci.* **2020**, *134*, 104410. [[CrossRef](#)]
20. Scholtes, L.; Donzé, F.-V. Modelling Progressive Failure in Fractured Rock Masses Using a 3D Discrete Element Method. *Int. J. Rock Mech. Min. Sci.* **2012**, *52*, 18–30. [[CrossRef](#)]
21. Popescu, F.D.; Radu, S.M.; Andras, A.; Brinas, I.; Marita, M.-O.; Radu, M.A.; Brinas, C.L. Stability Assessment of the Dam of a Tailings Pond Using Computer Modeling—Case Study: Coroiesti, Romania. *Appl. Sci.* **2024**, *14*, 268. [[CrossRef](#)]
22. Chen, X.; Liu, J.; Yuan, F.; Xu, L.; Ya-Hu, T.; Fang, J.-H. A Pseudo-Coupled Numerical Approach for Stability Analysis of Frozen Soil Slopes Based on Finite Element Limit Analysis Method. *Sci. Cold Arid Reg.* **2013**, *5*, 478–487.
23. Rasmussen, L.L.; Min, K.-B. Developments to the Bonded Block Modeling Technique for Discrete Element Simulation of Transversely Isotropic Rocks. *Int. J. Rock Mech. Min. Sci.* **2023**, *170*, 105518. [[CrossRef](#)]
24. Yuan, J.; Wang, C.; Liu, Z.; Lyu, J.; Lu, Y.; You, W.; Yan, J. Study on the Application of Finite Difference in Geological Mine Fault Groups: A Case Study. *Processes* **2024**, *12*, 1162. [[CrossRef](#)]
25. Gao, P.; Dong, G.; Chen, J.; Zhou, C.; Lin, M.; Zhang, W.; Yang, S. Study on Optimization of Stope Structural Parameters and Filling Scheme of Wawu Phosphate Mine in Yichang City, China. *Front. Earth Sci.* **2022**, *10*, 883572.
26. He, Z.-M.; Cao, P. Deformation and Stability Analysis of Underground Stope after Excavation Considering Strain Softening. *Zhongnan Daxue Xuebao (Ziran Kexue Ban)/J. Cent. South Univ. (Sci. Technol.)* **2008**, *39*, 641–646.
27. Schmid, C.J.; Newcomen, W.; Buchanan, M.; Corkum, A. Stability Evaluation of Stopes and Pillars at MAX Mine and Development of a Surpac-FLAC3D Model-Building Technique. In Proceedings of the ARMA US Rock Mechanics/Geomechanics Symposium, San Francisco, CA, USA, 23–26 June 2013.
28. Pino, J.; Gómez, R.; Marambio, E.; Miranda, R.; Delonca, A.; Suzuki, K. Three-Dimensional Effect of Stresses on Inclined Open Stope Mine Design. *Rock Mech. Rock Eng.* **2023**, *56*, 4647–4657. [[CrossRef](#)]
29. Wen, Z.; Tan, Y.; Han, Z.; Meng, F. Construction of Time-Space Structure Model of Deep Stope and Stability Analysis. *Pol. J. Environ. Stud.* **2016**, *25*, 2633–2639. [[CrossRef](#)]
30. Li, C.; Zhou, J.; Armaghani, D.J.; Li, X. Stability Analysis of Underground Mine Hard Rock Pillars via Combination of Finite Difference Methods, Neural Networks, and Monte Carlo Simulation Techniques. *Undergr. Space* **2021**, *6*, 379–395. [[CrossRef](#)]

31. Ren, Y.; Zhou, L.; Xing, J.; Qiu, J. Study on the Stope Stability of Jilongshan Gold Mine under the Condition of Empty Area around High Stress and Low Grade. *China Min. Mag.* **2019**, *28*, 119–123+129.
32. Idris, M.A.; Saiang, D.; Nordlund, E. Probabilistic Analysis of Open Stope Stability Using Numerical Modelling. *Int. J. Min. Miner. Eng.* **2011**, *3*, 194–219. [[CrossRef](#)]
33. An, H.; Fan, Y.; Liu, H.; Cheng, Y.; Song, Y. The State of the Art and New Insight into Combined Finite–Discrete Element Modelling of the Entire Rock Slope Failure Process. *Sustainability* **2022**, *14*, 4896. [[CrossRef](#)]
34. Chiloane, N.M.; Mgiba, C. Evaluation of Stope Stability in Deep Underground Mines Based on Stability Graphs and Numerical Simulations—A Comparison Study. In *New Challenges in Rock Mechanics and Rock Engineering*; CRC Press: Boca Raton, FL, USA, 2024; pp. 1018–1023.
35. Islavath, S.R.; Debasis, D. Stability Analysis of Underground Stope Pillars Using Three Dimensional Numerical Modelling Techniques. *Int. J. Min. Miner. Eng.* **2018**, *9*, 198–215. [[CrossRef](#)]
36. Tao, G.Q.; Ren, Q.Y.; Luo, H.; Liu, Z.D. Stability Analysis of Sublevel Caving Mining with No-Pillar Method. *Rock Soil Mech.* **2011**, *32*, 3768–3772.

Disclaimer/Publisher’s Note: The statements, opinions and data contained in all publications are solely those of the individual author(s) and contributor(s) and not of MDPI and/or the editor(s). MDPI and/or the editor(s) disclaim responsibility for any injury to people or property resulting from any ideas, methods, instructions or products referred to in the content.